# The Madden-Julian Oscillation in the ECHAM4/OPYC3 CGCM

Stefan Liess, Lennart Bengtsson and Klaus Arpe

Max-Planck-Institut für Meteorologie, Bundesstrasse 55,
D-20146 Hamburg, Germany

March 2001

submitted to
Climate Dynamics

ISSN 0937 – 1060

# Abstract

This study describes the ability of the coupled ECHAM4/OPYC3 atmosphere-ocean model, to represent the Madden-Julian oscillation (MJO). The ECMWF Reanalysis, radiosonde measurements at Singapore airport and NOAA satellite observations are used as reference.

We have analyzed 25 years of daily data of the coupled model. The Principal Oscillation Pattern analysis shows that the model is capable of simulating the MJO although it moves too fast and occurs too far eastward. The interannual variability of the simulated MJO is weaker than in observations and it reaches its maximum amplitude too late in the year in spring and summer instead of winter and spring as in the observations. Increasing the horizontal and vertical resolution of the atmospheric GCM seems to be an important step towards a better representation of the MJO.

We have also investigated selected events to examine the onset of the MJO. We suggest that the frictional wave-CISK theory plays the main role in the onset of the MJO. SST changes between 0.1 and 0.5K are associated with the passage of the MJO. It is also shown that the Westerly Wind Bursts are a result of the low-level convergence that follows the passage of the MJO.

# 1 Introduction

One of the most important phenomenons in the tropics on intraseasonal timescales is the Madden-Julian oscillation (MJO, Madden and Julian, 1971, 1972, 1994). It is an eastward propagating wave number one signal described by two zonal circulation cells. The original period of the MJO was thought to be 40-50 days, but numerous studies have broadened the period to cover a range of 30-60 days (e.g. Knutson and Weickmann, 1987). Therefore it is also known as the 30-60 day oscillation or intraseasonal oscillation.

The signal in the equatorial zonal wind is present throughout the entire tropical belt in the upper troposphere. Correct representation in the weather forecast models would lead to improved forecast skill also on shorter timescales (Lau and Chang, 1992; Waliser et al., 1999; Hendon et al., 2000). In the lower troposphere the MJO is confined to the Indian and western Pacific Ocean (e.g. Madden and Julian, 1972) where a maximum of variability in convection and large-scale circulation is found. Updrafts associated with deep convection in this region of warm SST are supposed to be the cause of the onset of the MJO. The resulting eastward propagation of super cloud clusters is forced by equatorial Kelvin wave propagation, with its structure modified by an associated forced Rossby wave in the eastern hemisphere that leads single cloud clusters to propagate westward within the super cloud cluster (e.g. Lau et al., 1989). The Kelvin wave propagates around the globe. Moisture supply from the Indian Ocean and the West Pacific warm pool reduces its propagation speed in this region (Wang, 1988; Jones and Weare, 1996; Wang and Xie, 1998).

Observational studies indicate that equatorial disturbances strongly favor the October through May period, specifically from December onwards (e.g. Wang and Rui, 1990b; Salby and Hendon, 1994). They exhibit strong variance over the Indian Ocean and south-east Asia but no pronounced eastward propagation along the equator during boreal summer (e.g. Rui and Wang, 1990). The dynamics of the MJO are strongly controlled by the dynamic effect of the equator through the change of algebraic sign of the planetary vorticity and by the thermodynamic effect of the thermal equator where SST is maximum. When the maximum SST moves away from the equator in the western Pacific, a situation similar to that of boreal summer, the growth rate of the unstable coupled mode decreases significantly (Wang and Rui, 1990a,b). The movement of the ITCZ, which is quite symmetric around the equator in that region (Philander et al., 1996) is strongly related to the SST. It leads to enhanced convection during the equinoxes. The MJO is most active during this period (Salby et al., 1994). Even aquaplanet-models represent an MJO-type oscillation (e.g. Hayashi and Sumi, 1986; Swinbank et al., 1988; Flatau et al., 1997).

Hence the MJO occurs in the monsoon region, its eastward propagation is affected by the planetary monsoon and the related Hadley circulation. Wang and Rui (1990b) describe the northward propagating clouds of the Indian summer monsoon and the eastward propagating MJO mode as independent from each other but during the transition from monsoon type circulation to MJO type circulation they define the interaction as an EN (east-north) mode. The onset of the Australian summer monsoon is defined as the first occurrence of 850hPa westerlies with a speed of at least 5 m $s^{-1}$ and a rainfall rate of at least 5 mm $day^{-1}$ in Darwin and this is strongly associated with the convective phase within the first MJO per season that reaches northern Australia (Hendon and Liebmann, 1990a,b).

The origin of the propagation of the MJO has been a subject of many studies (e.g. Knutson and Weickmann, 1987; Lau and Peng, 1987; Wang and Rui, 1990a) that are briefly reviewed by Madden and Julian (1994). The three main theories of theses studies are the frictional wave-CISK (e.g. Lindzen, 1974; Wang, 1988; Salby et al., 1994), the evaporation-wind feedback, also called wind-induced surface heat exchange (WISHE, e.g. Neelin et al., 1987; Emanuel, 1987) and the air-sea interaction that takes diabatic heating, entrainment cooling and thermocline variations in the ocean into account as reasons for the wave propagation (e.g. Krishnamurti et al., 1988; Lau and Sui, 1997; Wang and Xie, 1998). These theories are reviewed in detail by Flatau et al. (1997).

Westerly Wind Bursts (WWB) seem to be a consequence of the MJO activity (e.g. Lau et al., 1989; Nakazawa, 1999). They occur to the west of the enhanced low-level convergence resulting from the onset of the MJO. To the east of this convergence enhanced easterlies can be found. WWBs can significantly modify the structure of the thermocline in the equatorial Pacific Ocean on the intraseasonal time scale (e.g. McPhaden and Taft, 1988; Kessler et al., 1995; Zhang, 1997) and by this they seem to play an important role for the onset of an El Niño (Weickmann, 1991; Kessler et al., 1995; Nakazawa, 1999; van Oldenborgh, 2000).

Many studies with atmospheric general circulation models (AGCM) have been undertaken to analyze the MJO (e.g. Hayashi and Golder, 1993). Slingo et al. (1996) compared the ability of 15 AGCMs to simulate the MJO. Gualdi et al. (1997) analyzed different versions of the ECHAM AGCM. Since the MJO is a coupled air-sea phenomenon, the necessity to study it with coupled atmosphere-ocean GCMs (CGCM) is evident (Waliser et al., 1999). In this study, the capability of the CGCM ECHAM4/OPYC3 (Roeckner et al., 1996; Bacher et al., 1998) to represent the MJO is investigated. Chapter 2 deals with the characteristics of the MJO as obtained from the ECMWF Reanalysis data and observations. The representation of the MJO in the CGCM ECHAM4/OPYC3 is depicted in Chapter 3. These results are discussed in Chapters 4 and 5.

# 2 Observations

The MJO is analyzed with daily ECMWF reanalysis data at T106 horizontal resolution and 31 vertical layers as well as pentad NOAA OLR data (Liebmann and Smith, 1996) at 2.5°×2.5° horizontal resolution covering the period 1984 to 1988 and radiosonde observations from Singapore airport. 15-90 day bandpass filtered ECMWF 200 hPa velocity potential between 10°N and 10°S are used to perform a Principal Oscillation Pattern (POP) analysis (Hasselmann, 1988; von Storch et al., 1988, 1995). The seasonal cycle of the data was removed prior to POP analysis.

The explained variance of this oscillation amounts to 23.8%. Fig. 1 illustrates the squared coherence spectrum of the POP coefficients of the leading POP mode (e.g. von Storch and Zwiers, 1999). Only periods between 10 and 100 days are depicted, since periods outside this domain are too much influenced by the bandpass filter. Highest coherence is found at a period of 48 days. A secondary peak is detectable near the 20 days period, which might be the mode described by Hayashi and Golder (1993). At both peaks the relative phase of the complex POP coefficient appears to be around -90°(not shown), indicating that the imaginary part leads the real part, as theoretically expected (Gallagher et al., 1991; von Storch and Zwiers, 1999). This mode has an $e$-folding time of 56 days.

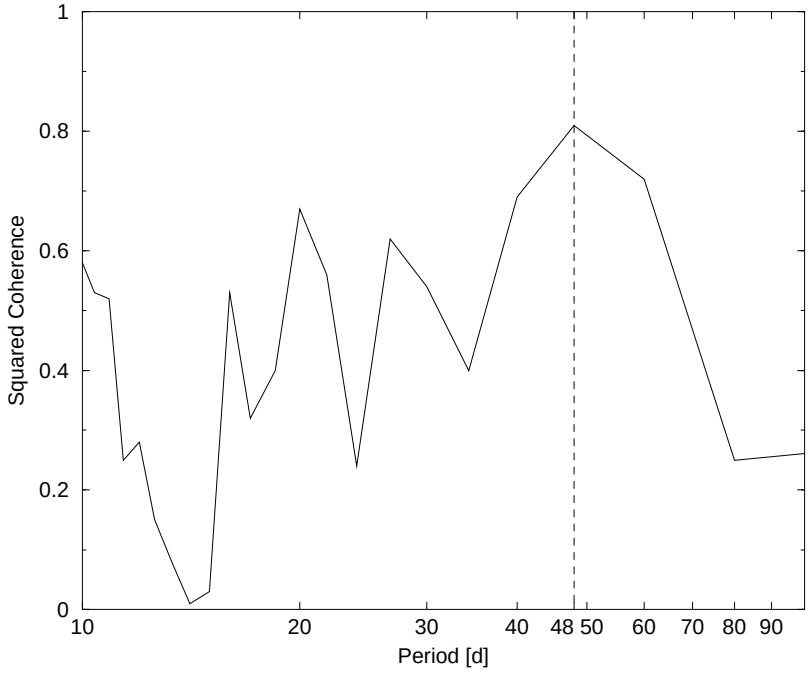


Figure 1: Squared coherence spectrum of the POP coefficients of the leading POP mode.

Following von Storch et al. (1988) and Gualdi et al. (1997), the dominant complex POP coefficients are used to obtain eight composites of 45° segments. Each of them represents a different phase of the oscillation. Only values with an amplitude larger than the mean

amplitude plus 0.8 times the standard deviation are considered. The running mean over a 5-day window where the two adjacent dates of each value are taken into account is used to accentuate the mean state of each segment.

For each of the eight phases Figs. 2 and 3 show the unfiltered 200 hPa velocity potential anomaly as contour lines (with negative values dashed) and the NOAA OLR anomaly in Fig. 2 and the reanalysis OLR anomaly in Fig. 3, respectively. Strong negative OLR anomalies are shaded indicating deep convection. The variance of OLR anomaly is slightly weaker in the reanalysis than in the satellite data, but the MJO pattern is well represented in both datasets. The panels represent a kind of pseudo-Hovmöller diagram with time running from top to bottom.

The leading POP mode resembles the oscillation described by Madden and Julian (1971) and other authors. The onset, growing, eastward propagation and decay of the OLR anomaly is consistent with those presented in Fig. 16 of Madden and Julian (1972). Also the velocity potential anomaly representing large-scale convergence shows slow propagation in phase with the OLR anomaly during the convective regime and faster propagation during the dry regime. A secondary maximum of convection and large-scale divergence occurs over eastern tropical South America (panel seven).

For further analysis of the MJO it is important to find an index that describes the activity of the MJO. Many indices have been discussed before, e.g. the power spectrum of eastward propagating OLR waves with wavenumbers 1 to 3 described by Salby and Hendon (1994), the variance within a 100-day moving window of 200 hPa zonal mean zonal wind established by Slingo et al. (1996, 1999) and the 100-day running mean of the squared amplitude of the POP coefficients (Gualdi et al., 1999). These indices are very useful in representing the interannual variability in the activity of the MJO, but for our study an index that describes each single oscillation is needed.

An EOF analysis of the 15-90 day bandpass filtered 200 hPa velocity potential anomaly between 10°N and 10°S is performed. The first EOF represents the maximum activity of the MJO with negative velocity potential anomaly over the eastern Indian Ocean and the western Pacific (Fig. 4). It explains 37.0% of the total variance. Fig. 5 shows the corresponding first principal component (PC1). Please note, that the leading EOF mode cannot be regarded as an index of the full MJO activity, since one EOF cannot describe the propagating features.

The syntheses of the individual MJO events are somewhat complicated because of the great diversity of the phenomenon (Wang and Rui, 1990b), e.g. the propagation speed differs from event to event. Averaging over many MJO events might lead to deficient evidences when local disturbances are compared that might belong to different MJO events.

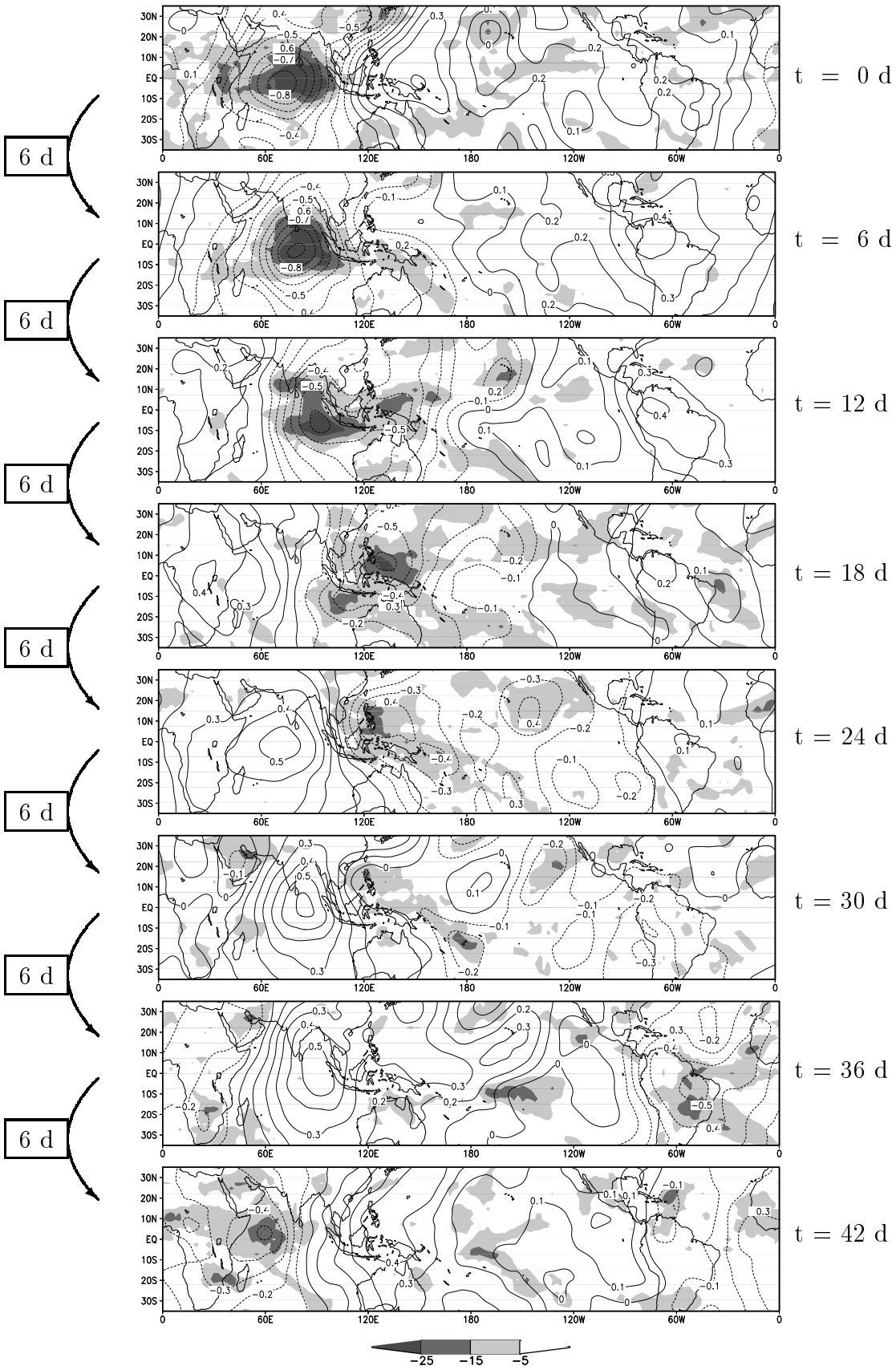


Figure 2: Pseudo-Hovmöller diagrams of NOAA OLR anomaly [W $m^{-2}$] and reanalysis 200 hPa velocity potential anomaly [$10^7$ $m^2 s^{-1}$]. Negative OLR anomaly (shaded) indicates deep convection and negative velocity potential anomaly (dotted) indicates large-scale divergence. Arrows on the left and the scale on the right point out the time step between the panels as derived by the POP analysis.

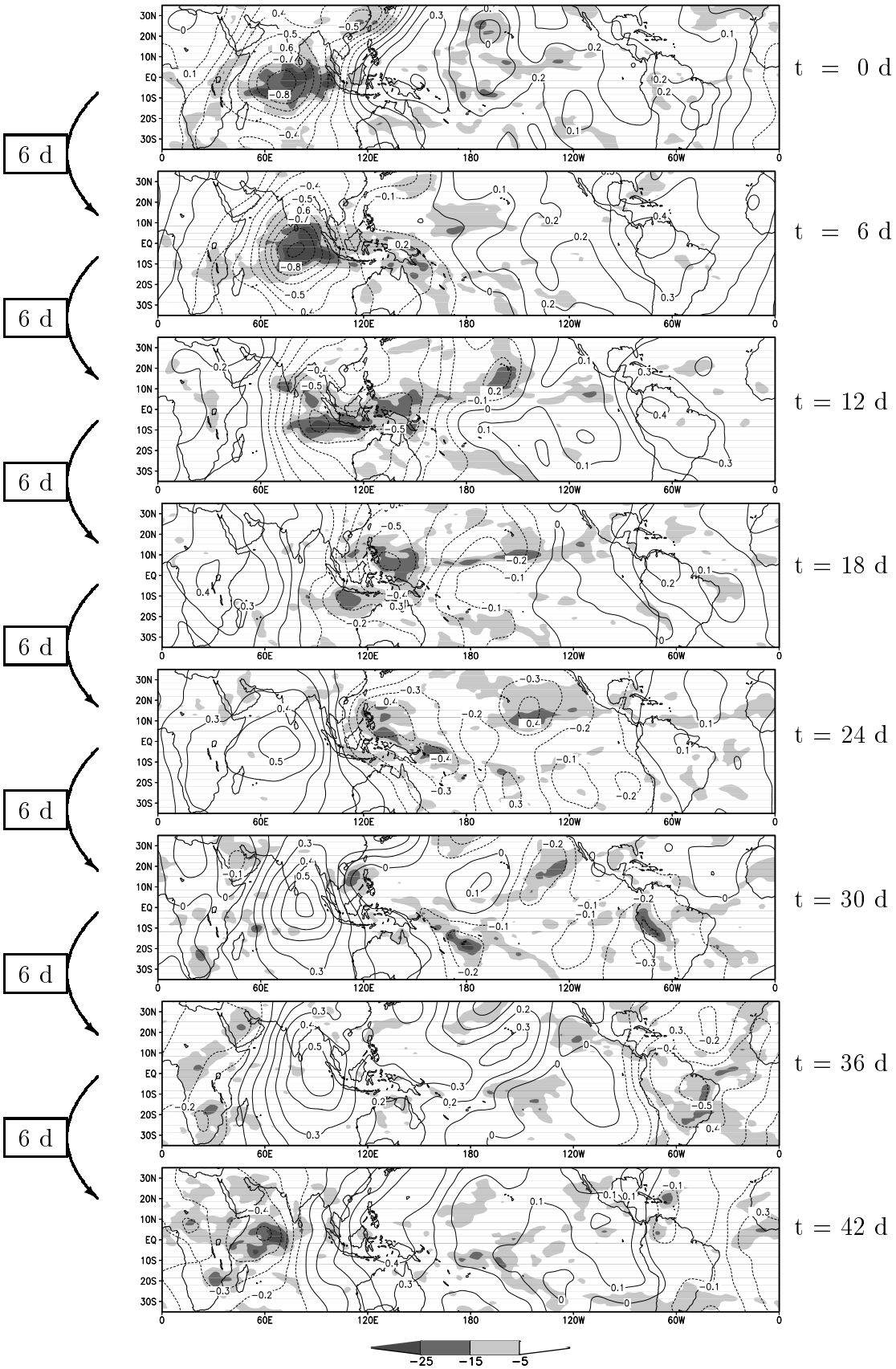


Figure 3: As Fig. 2, but for reanalysis OLR.

For this reason a case study with only one MJO event seems to be more appropriate. The maximum of PC1 occurs at the 23rd of March 1988 and the corresponding MJO is taken for the case study. This is consistent with the studies by Salby and Hendon (1994), Slingo et al. (1999) and Gualdi et al. (1999), who also detected strong MJO activity during spring 1988. The MJO event considered here is a well known event, also analyzed by Matthews et al. (1996) investigating the interaction of the SPCZ and MJO.

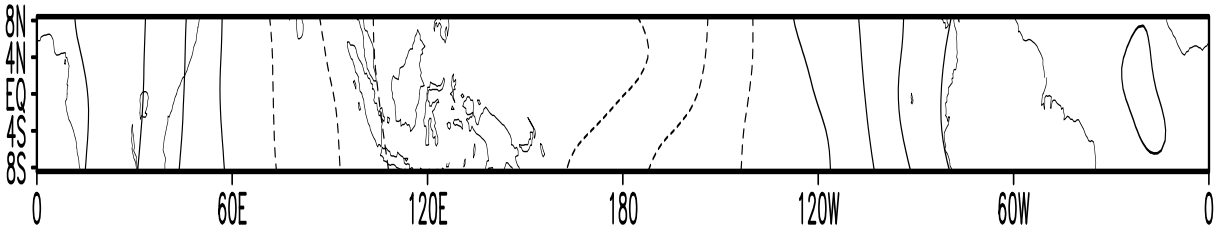


Figure 4: ECMWF first EOF of 200 hPa velocity potential anomaly in the equatorial region. Contour interval is 0.005, negative values are dashed and the pattern explains 37.0% of the total variance.

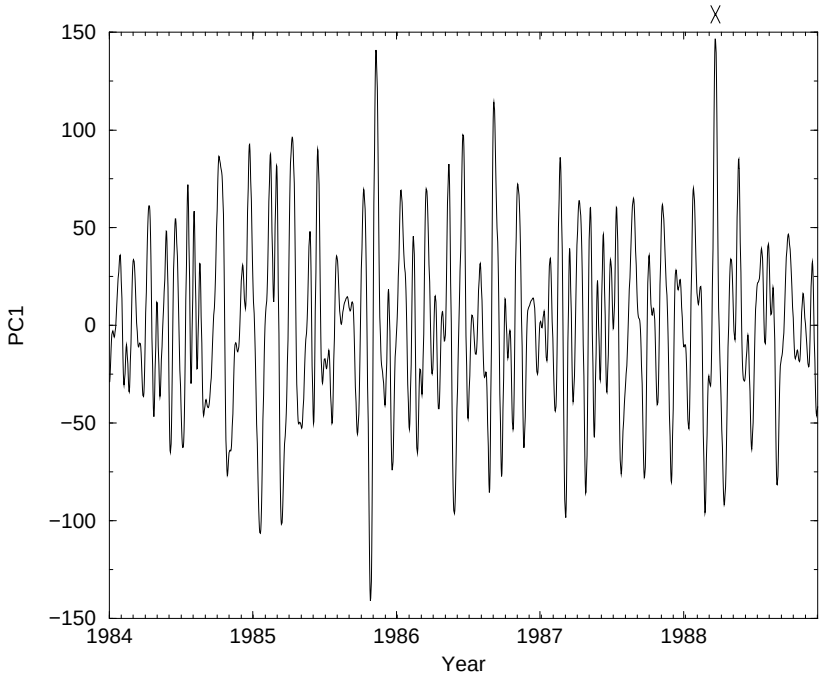


Figure 5: ECMWF PC1 which is used as an index of the activity of the MJO. X marks the maximum at the 23rd of March 1988 as an identifier for a typical MJO. A high value of the PC1 describes a strong MJO activity (Slingo et al., 1999).

The EOF index reflects the interannual variability very well compared to the $\overline{u_{200}}$-variance index (Fig. 6) by Slingo et al. (1999) and the POP-coefficient index (Fig. 7) by Gualdi et al. (1999). The winters 1985, 1986 and 1988 exhibit strong MJO activity, whereas during the winters of 1984 and 1987 it was considerably weaker. The weak MJO activity during 1984 might be related to the easterly phase of the QBO (not shown). Westward propagating cloud clusters dominate over the eastward propagating super cloud clusters. The uncommon westward propagation was likewise observed by Wang and Rui (1990b). Salby and Hendon (1994) also found MJO activity in 1987, which is shifted slightly to the north.

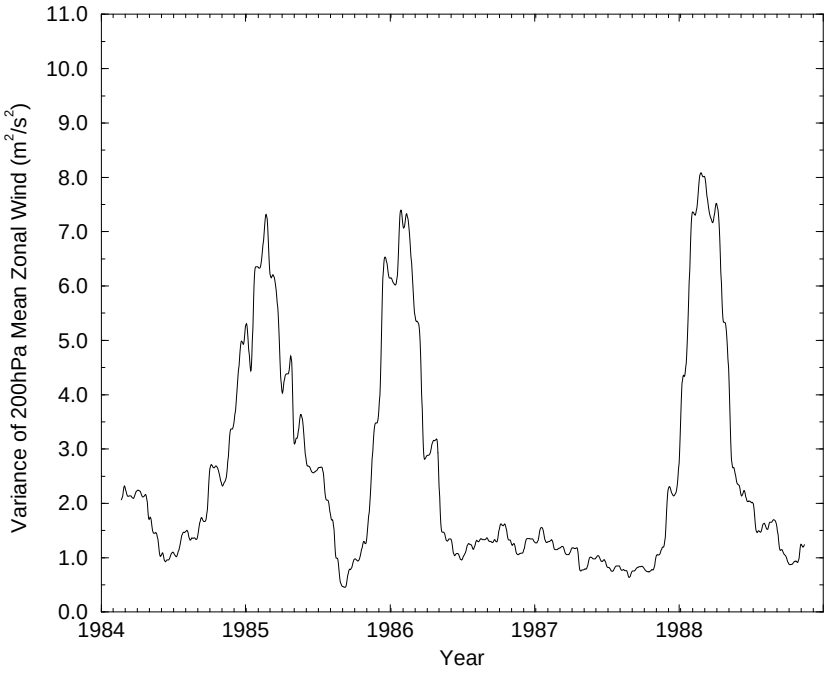


Figure 6: ECMWF $\overline{u_{200}}$-variance averaged between 10°N and 10°S within a 100-day moving window, an index for the interannual variability of the MJO activity.

The weak MJO activity during 1987 is related to weak convective activity over the Indian Ocean due to the El Niño occuring at that time, as suggested by Gualdi et al. (1999). Strong MJO activity occurs prior to the La Niña in 1988, as indicated by the NINO3 SSTA (Fig. 8). The two vertical lines mark 20 days before and 40 days after the MJO event, respectively. The MJO activity is strongest at the time of steepest NINO3 SSTA decrease. The teleconnections associated with the 1988 La Niña and the westward shift of the west Pacific warm pool due to a downwelling Rossby wave is described by Picaut and Delcroix (1995).

The equatorial SST is at a maximum in northern spring when the trade winds are relaxed (Philander, 1990). The corresponding increase in tropical convection leads to the strong MJO activity in the Indian Ocean. During the mature phase of La Niña during northern

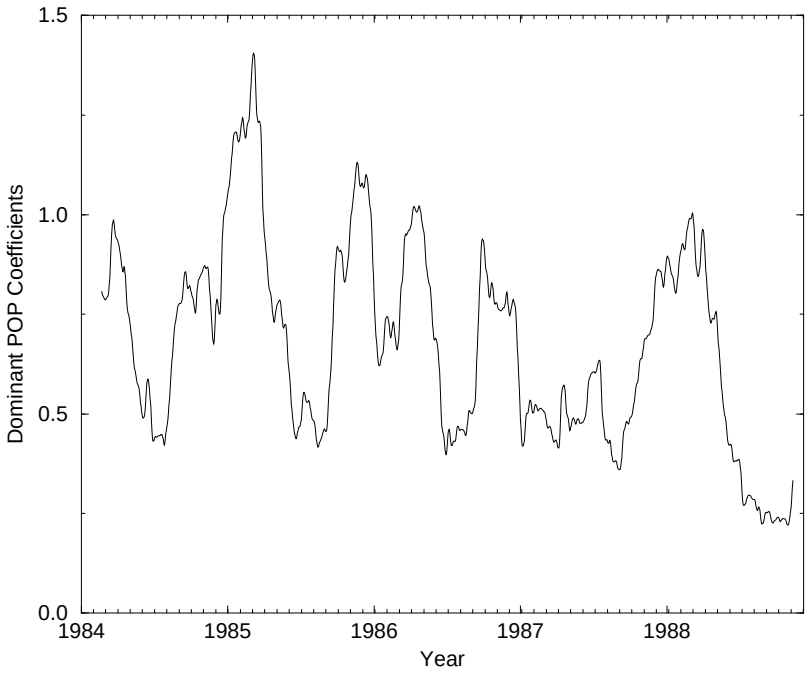


Figure 7: ECMWF 100-day running mean of the squared amplitude of the POP coefficients, reflecting the interannual variability of the MJO activity.

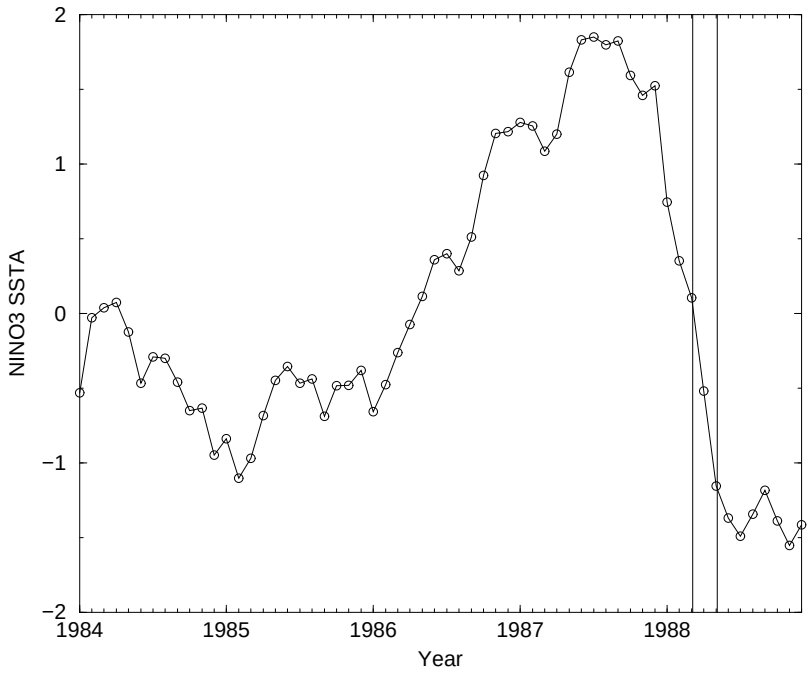


Figure 8: Monthly mean NINO3 SSTAs [K] and the PC1 maximum (20 days before and 40 days after the maximum, indicated by the two vertical lines).

summer after the onset of the monsoon, the ITCZ is shifted north of the equator (Fig. 9). Wang and Rui (1990a) showed that the growth rate of equatorial Kelvin waves decreases substantially, when the SST maximum shifts northward to 7.5° N. At that time the deep convection occurs too far north of the equator and therefore the MJO activity decreases (Salby et al., 1994).

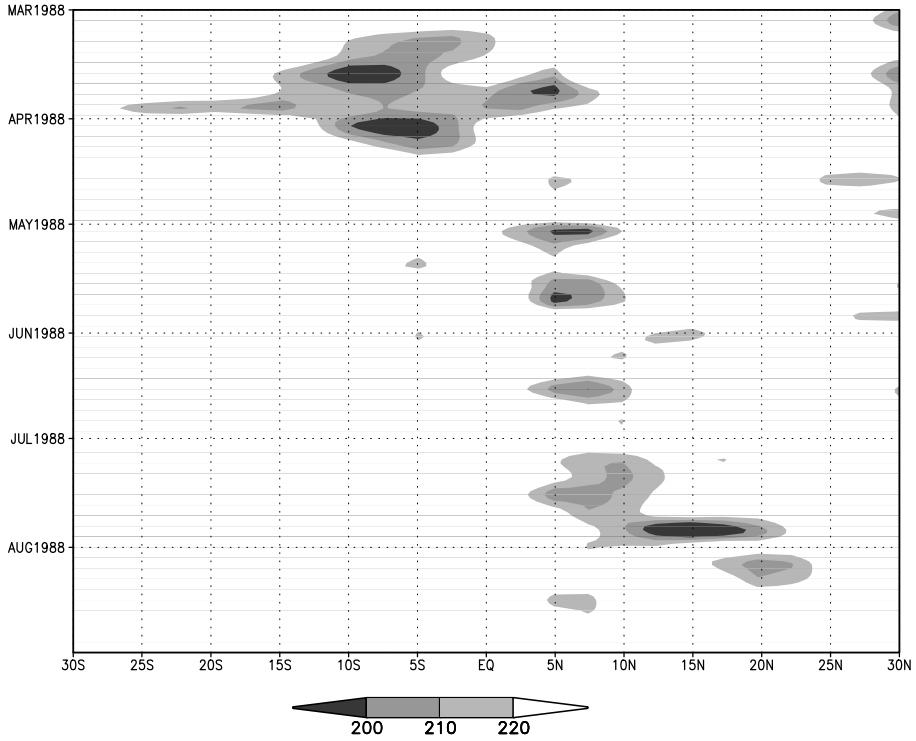


Figure 9: Time-latitude Hovmöller diagram of NOAA OLR [W $m^{-2}$] over the West Pacific warm pool averaged between 120°E and 180°. Dark shading indicates deep convection.

The MJO is best observed in the zonal wind field. According to numerical experiments by Lau et al. (1989) and observational studies by Rui and Wang (1990) and Jones and Weare (1996) upper tropospheric easterlies increase during the passage of the convection anomaly and lower troposphere westerlies have a maximum slightly after the passage, although the low-level convergence leads the convective anomaly in the mature phase of the MJO, which is consistent with the influence of the equatorial Rossby wave (Matsuno, 1966; Wheeler et al., 2000). A comparison of reanalysis data to zonal wind observations from Changi airport at 1°22'N and 103°59'E in Singapore shows that the passage of the MJO is represented in both datasets (Fig. 10). The upper-level easterlies strongly increase due to the convective updrafts. The lower-level zonal wind field contains the structure of a typical WWB due to the resulting low-level convergence. A lag-correlation analysis for the time series of the low-level zonal wind to that of the upper-level zonal wind yields a lag of 3.5 days for the observations and 3.0 days for the reanalysis at a correlation of -0.66 and -0.74 respectively. This indicates that the characteristic propagation of the MJO is well represented in the reanalysis data.

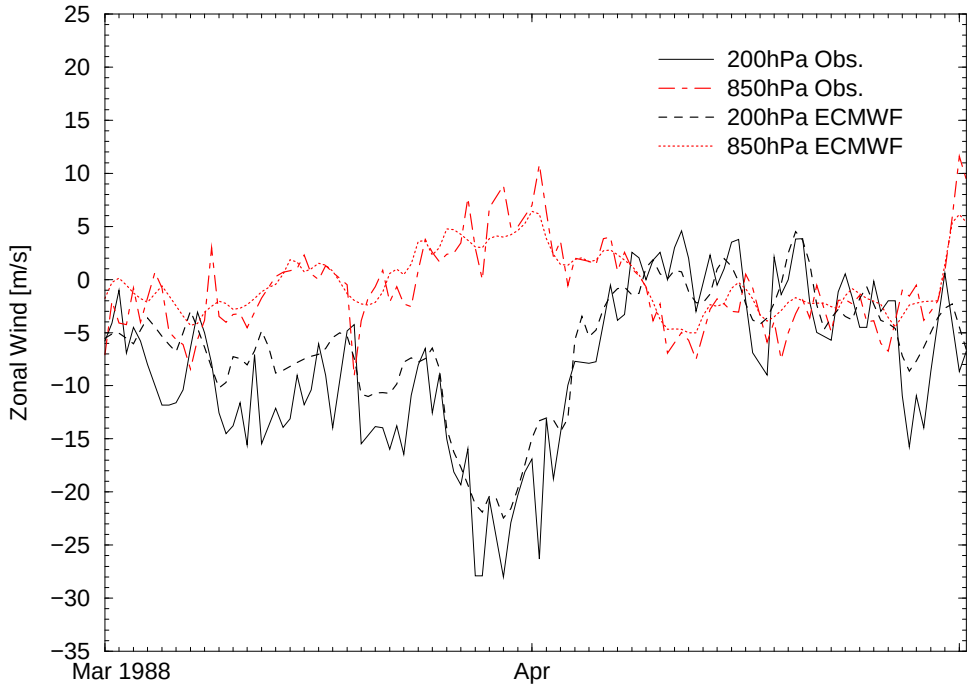


Figure 10: Time series of zonal wind [m $s^{-1}$] in 200 hPa and 850 hPa: Observations from Changi airport in Singapore and ECMWF Reanalysis in the corresponding grid point.

Fig. 11 shows the zonal wind and the cloud cover fraction in an equatorial zonal cross section on March 23rd 1988 (left) and also the cloud cover fraction as mean values of the equatorial West Pacific (right) to demonstrate the trimodal distribution of convective clouds within the Tropics as described by Johnson et al. (1999). The low- and mid-level convective clouds moisten the atmosphere whereas deep convection dries the atmosphere due to heavy rainfall and descending air between the convective plumes (Inness et al., 2001). The pattern of the zonal wind resembles the one simulated by Lau et al. (1989) in their Fig. 9c, although the WWB is not well developed on March 23rd 1988, yet. The increased upper-tropospheric easterlies shuffle some cloud clusters to the west of the super cloud cluster due to initiated Rossby waves (Lau et al., 1989). A consequence is an increased solar insolation and increased SST to the east of the convection. The resulting meridional moisture flux convergence leads to the eastward propagation of the super cloud cluster, which is consistent to the wave-CISK and air-sea interaction theory (Flatau et al., 1997).

In addition to the POP analysis and the general description of the detected MJO event, longitude-time Hovmöller diagrams are used to analyze the onset and characteristics of the MJO in time and space. The data of 20 days before and 40 days after the maximum of PC1 are depicted meridionally averaged between 10°N and 10°S. Fig. 12 presents the negative OLR anomalies for NOAA data and ECMWF Reanalysis data, respectively. The maximum of convection is indicated by minimum OLR. The NOAA data are coarser

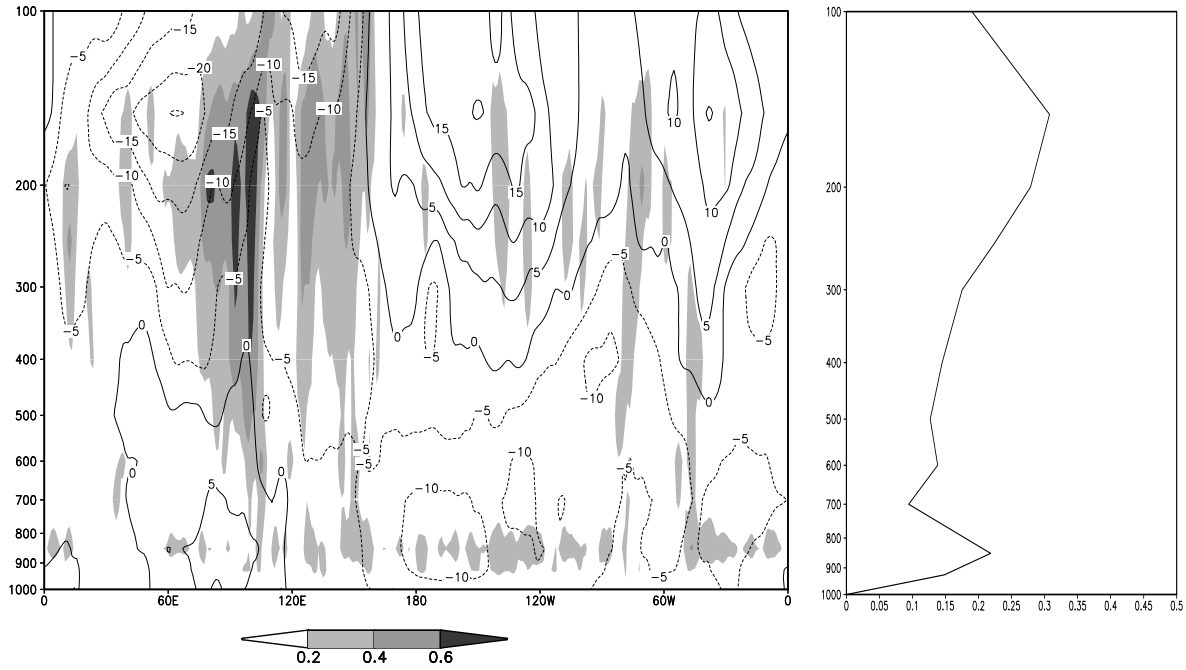


Figure 11: ECMWF cloud cover fraction at March 23rd 1988. Left: Zonal section of cloud cover fraction averaged between 10°N and 10°S (shaded) and zonal wind [m $s^{-1}$] (contours). Right: West Pacific region averaged between 10°N, 10°S, 120°E and 180°.

in time, because the daily data are interpolated from pentads. Nevertheless, the main characteristics are still clearly visible. The super cloud cluster propagates eastward over the Indian Ocean and the West Pacific between 60°E and 150°E during March 16th to 26th for the detected MJO event and during April 18th to May 1st for a subsequent MJO event. The decay of convection for the detected MJO between 150°E and 180° takes longer and has less eastward propagation in the reanalysis data than in the observations. The weak convection anomalies at about 70°W and 0° over the South American and West African rainforest, respectively, are standing in nature.

The local SST increases before the passage of the MJO convection center and decreases after its passage, due to enhanced surface shortwave flux to the east of the convection and enhanced latent heat flux coincident with the convection and to the west of it (Lau and Sui, 1997; Waliser et al., 1999). High SST to the east of the convection increases the meridional moisture flux convergence which activates the wave-CISK mechanism and leads to the eastward propagation of the super cloud cluster.

To highlight the small-scale variations of SST, only the Indian Ocean and the West Pacific regions are plotted in Fig. 13. The two panels depict the SST pattern 10 days before the maximum MJO activity (13th of March 1988) and at the maximum of MJO activity (23rd of March 1988). The SST decreases in the western and southern Indian Ocean and it increases in the north-eastern Indian Ocean and the West Pacific warm pool, as

indicated by the 29.5°C isotherm. The change of SST associated with the passage of an MJO is in the range of 0.1 to 0.5 K, consistent with observations from TOGA/TAO (Kessler et al., 1995; Jones et al., 1998).

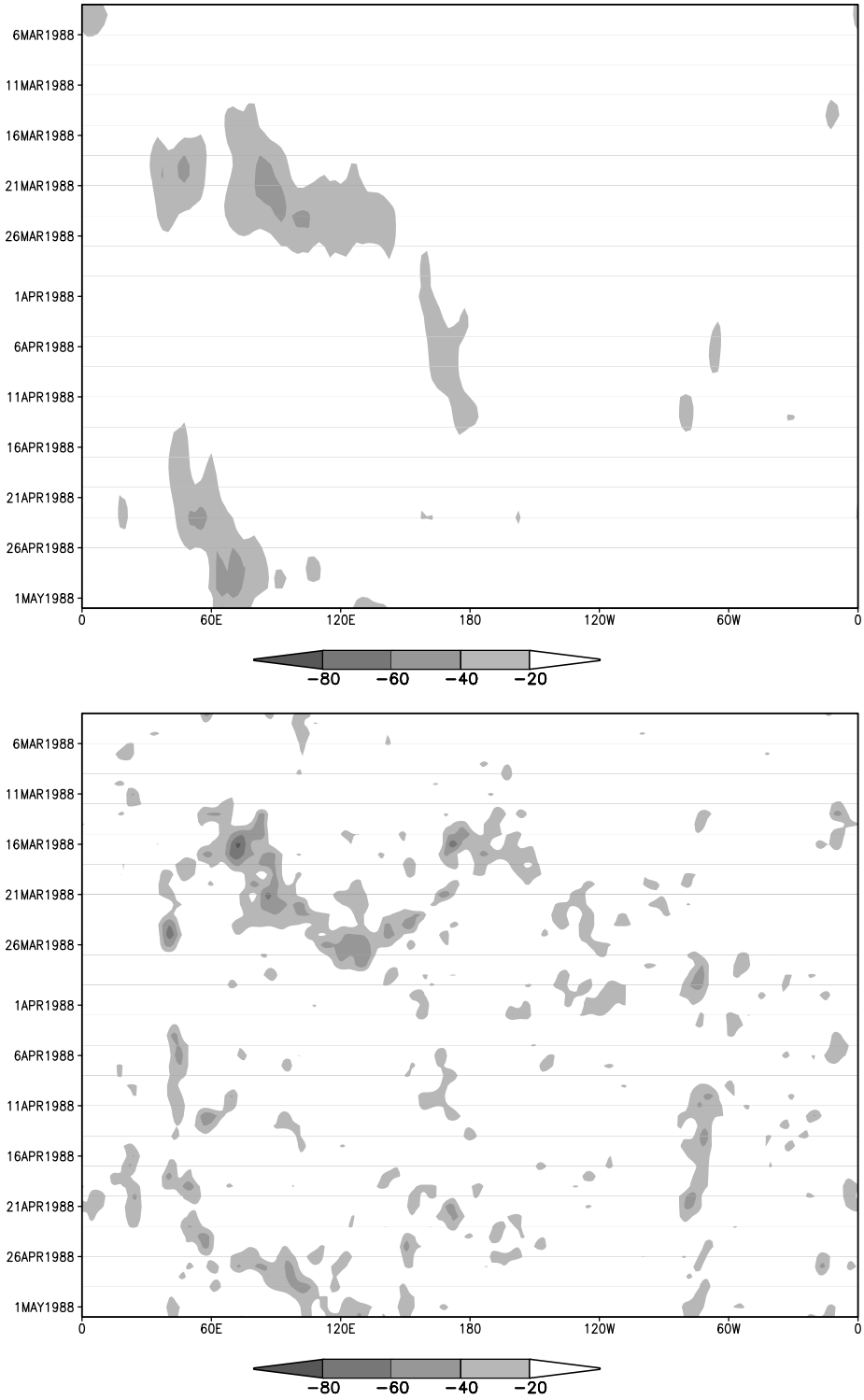


Figure 12: NOAA OLR anomaly (top) and ECMWF OLR anomaly (bottom) [W $m^{-2}$] averaged between 10°N and 10°S.

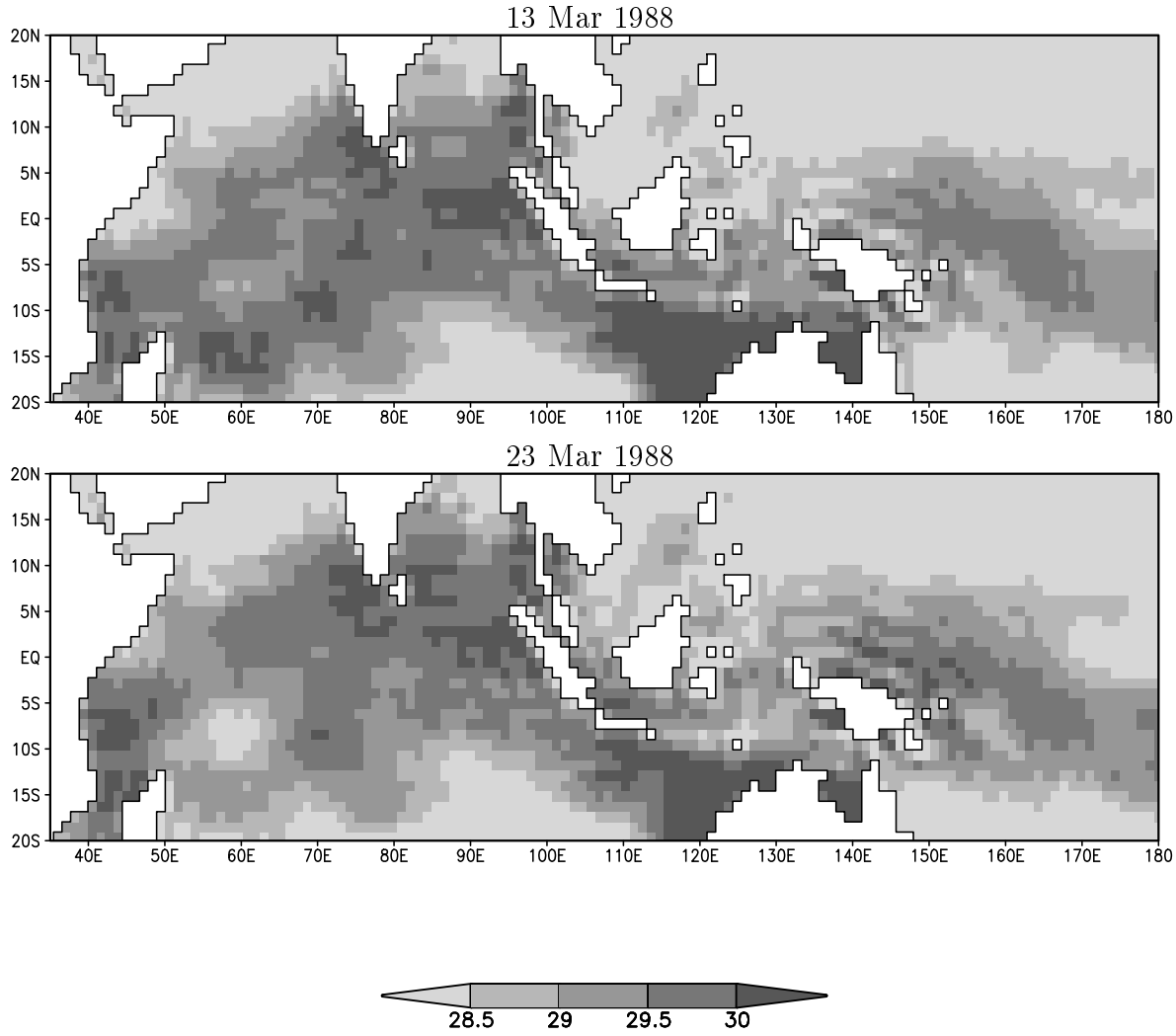


Figure 13: ECMWF SST [°C] with corresponding land-sea mask at March 13th (top) and March 23rd (bottom) 1988.

Fig. 14 describes the large-scale dynamics at 200 hPa and in the boundary layer. Shown are velocity potential anomalies averaged between 10°N and 10°S. The maximum of 200 hPa large-scale divergence occurs during the maximum in convection (Fig. 12). The maximum of lower-troposphere large-scale convergence lags the activity in the upper troposphere in time but leads it in space, i.e. its maximum is shifted eastward, as observed by e.g. Jones and Weare (1996). The increase occurs at first at 850 hPa, then at 925 hPa and a few days later at 1000 hPa indicating that the wave-CISK mechanism is active in the boundary layer. SST and velocity potential anomalies are in phase in the eastern hemisphere and out of phase elsewhere, because the propagation speed of the MJO increases in the eastern Pacific and the propagation of the changes in SST slows down and vanishes near the date line.

Fig. 15 implies that the WWBs between 60°E and 120°E occur slightly after the passage of the MJO due to the low-level convergence, which is consistent with observations by Nakazawa (1999).

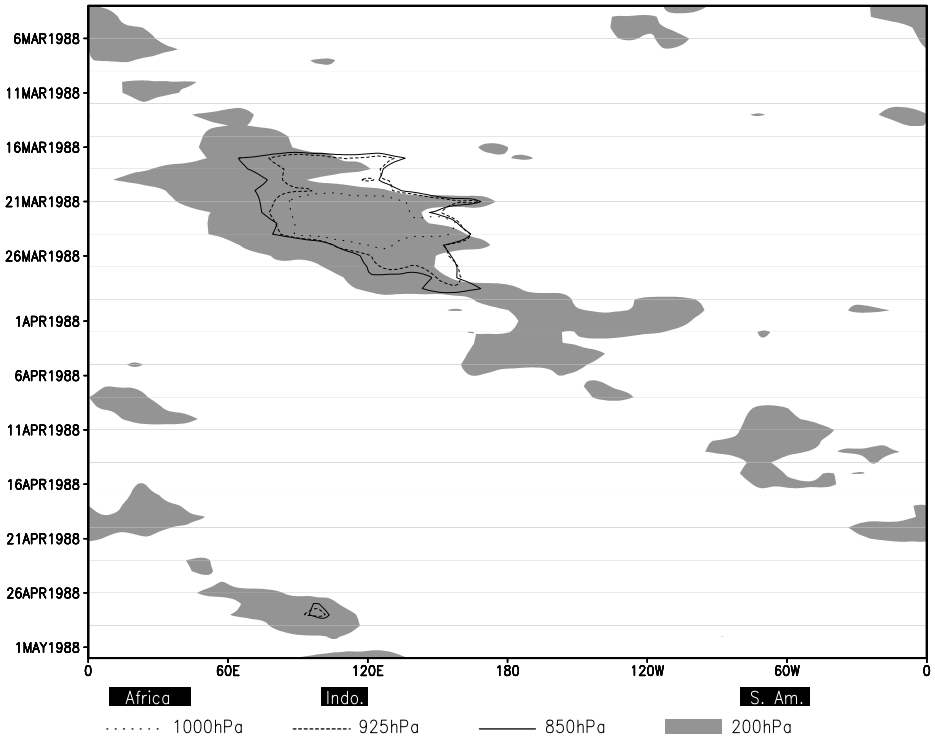


Figure 14: ECMWF velocity potential anomalies averaged between 10°N and 10°S. Shaded: negative values less than -5·10$^6$ m$^2$ s$^{-1}$ at 200 hPa height, contours: 5·10$^6$ m$^2$ s$^{-1}$ isolines at the specified heights.

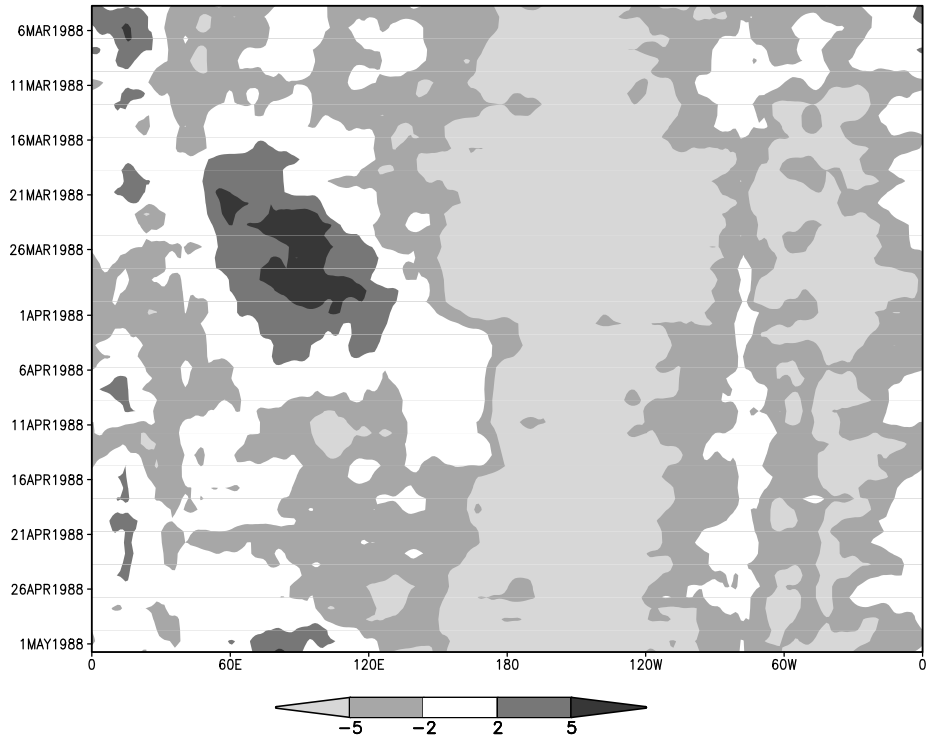


Figure 15: ECMWF 850 hPa zonal wind [m s$^{-1}$] averaged between 10°N and 10°S.

# 3 Model Results

The AGCM ECHAM4 at T42 horizontal resolution has been coupled to the OGCM OPYC3 (Roeckner et al., 1996; Bacher et al., 1998). Daily data of 25 CGCM-years (251 to 275) are analyzed concerning the ability to simulate the MJO. The oscillation period of the dominant POP mode is about 27 days (Fig 16) with an $e$-folding time of more than 60 days. This wavenumber one oscillation describes 54.7% of the explained variance which is considerably more than the variance explained by the corresponding leading POP mode in the reanalysis data.

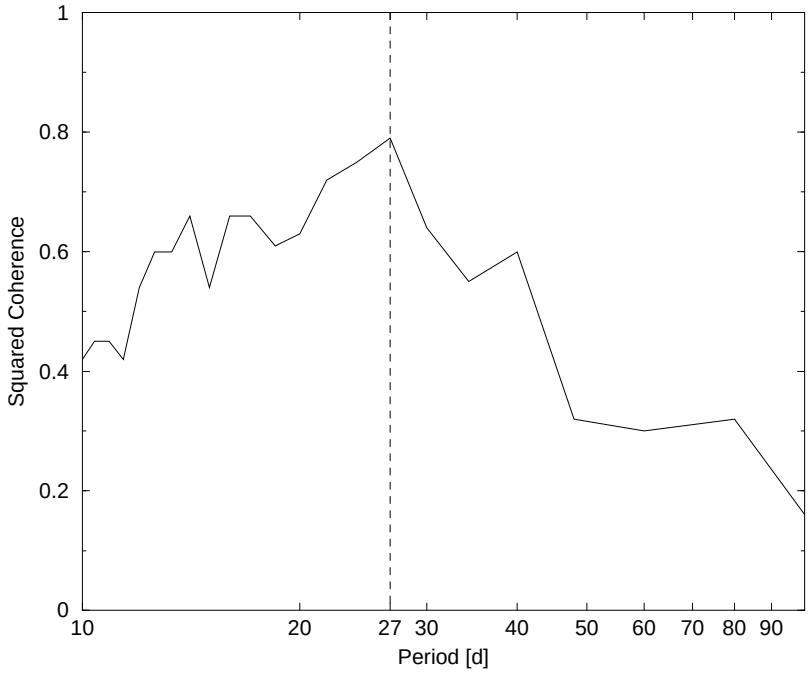


Figure 16: ECHAM4/OPCY3 squared coherence spectrum of the POP coefficients of the leading POP mode.

Fig. 17 describes the result of the POP analysis, similar to that in the previous chapter. The time step from one panel to the next is about 3.4 days. The model reproduces a more distinct oscillation than that found in the observations. The onset, growing and eastward propagation are simulated at the right time during the convective regime. However, a gap of convection occurs over the maritime continent in panels one and two. The western super cloud cluster forms a standing oscillation in the velocity potential anomaly over the Indian Ocean indicated by the local minimum in phase one and two and the local maximum in phase five, whereas a study by Zhang and Hendon (1997) indicates that the observed MJO is not dominated by a standing oscillation. The super cloud cluster over the West Pacific warm pool grows and propagates eastward. The eastward propagation, however, occurs too far eastward, and the propagation of the super cloud cluster also fades away too far eastward over the eastern Pacific. This splitting of the super cloud cluster

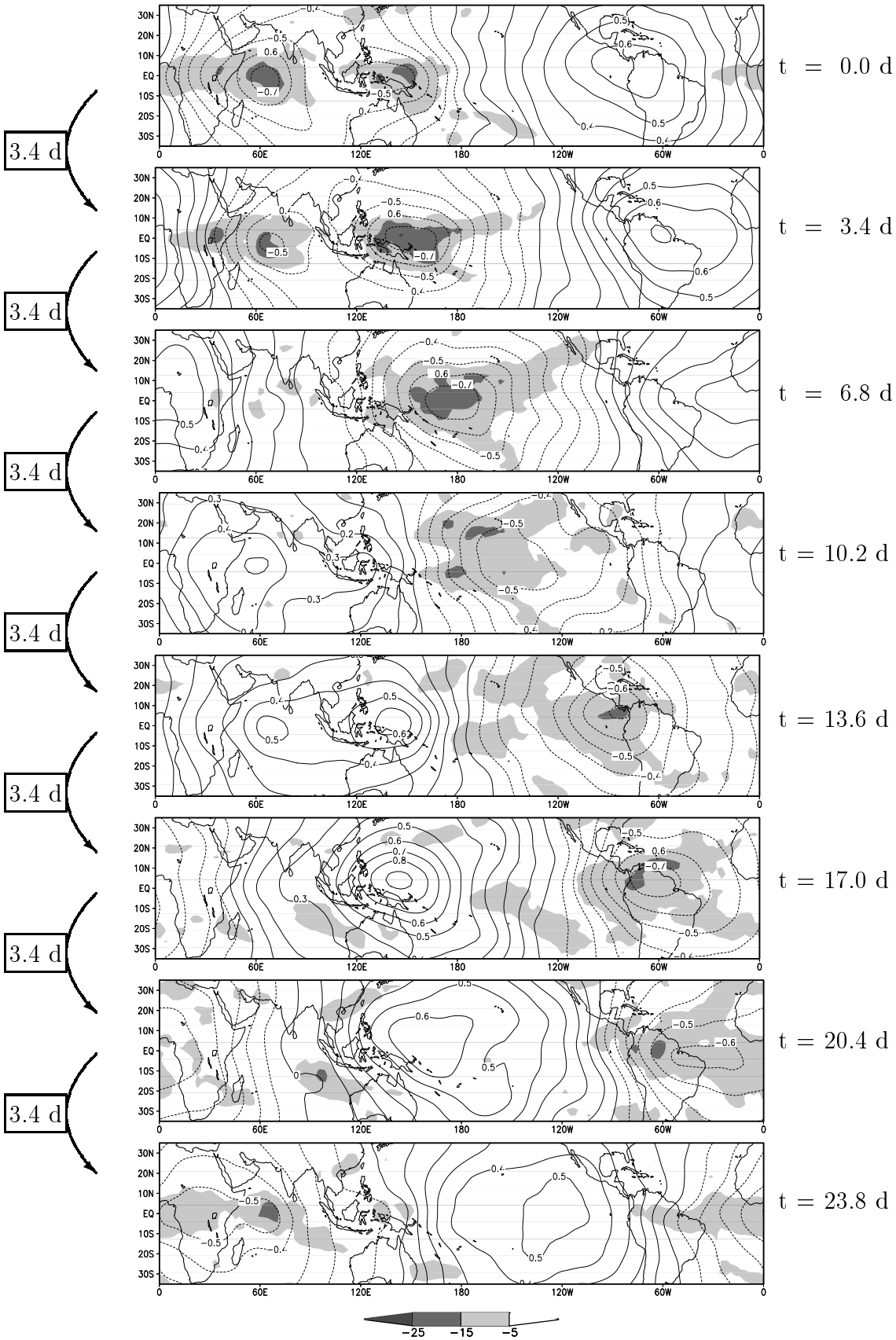


Figure 17: As Fig. 2, but for ECHAM4/OPCY3.

seems to be due to the coarse horizontal resolution and the consequential broadening of land points in this area. The secondary maximum of the amplitude over the South American rainforest is stronger than in the observations, which is a systematic error in the ECHAM4 model. The velocity potential anomaly is in all phases in phase with the convection, so it is not possible to distinguish between a convective and a dry regime very clearly. In all phases the two propagating cells have about the same sizes and propagation speeds.

As in the reanalysis, the first EOF describes the onset of the dominant mode of the MJO (Fig. 18). Its explained variance amounts to 35.6% and the pattern resembles the one from the reanalysis data (Fig. 4). Fig 19 shows the corresponding time series of PC1. It is confined to the years 270 to 274 for the sake of clarity. The absolute maximum occurs at the 24th of March in the model year 274. The interannual variability of the MJO activity is simulated reasonably well by the model (Figs. 20 and 21), but the main activity occurs too late in the year in spring and summer instead of winter and spring as observed.

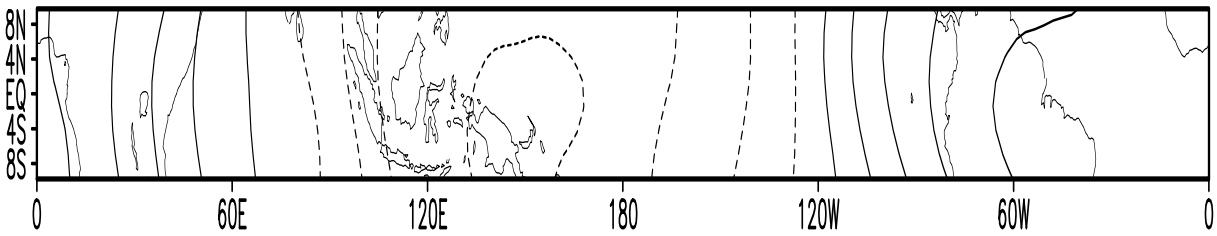


Figure 18: ECHAM4/OPYC3 first EOF of 200 hPa velocity potential anomaly in the equatorial region. Contour interval is 0.01, negative values are dashed and the pattern explains 35.6% of the total variance.

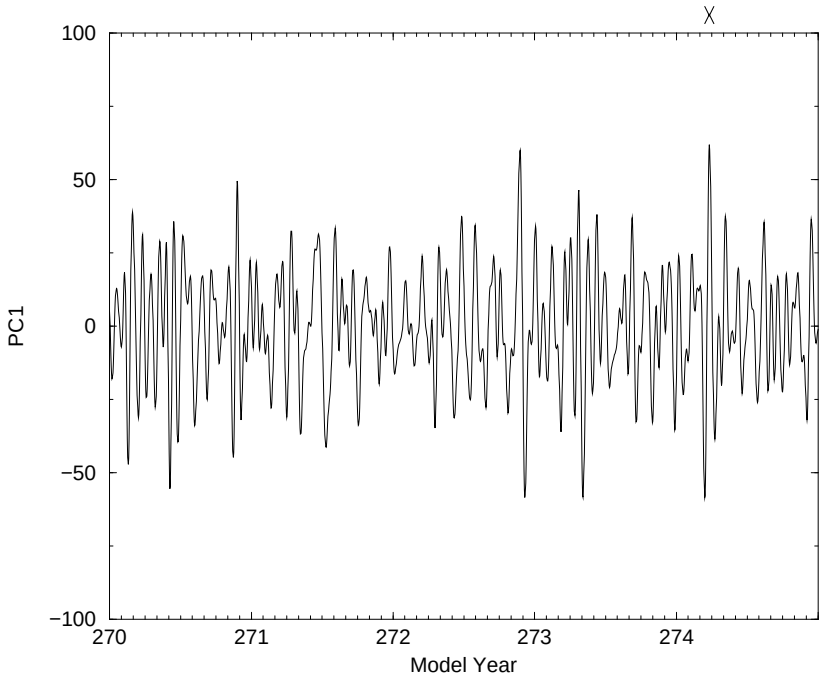


Figure 19: ECHAM4/OPYC3 PC1 as an index of the activity of the MJO. X marks the maximum at the 24th of March 274. This event is used in the case study.

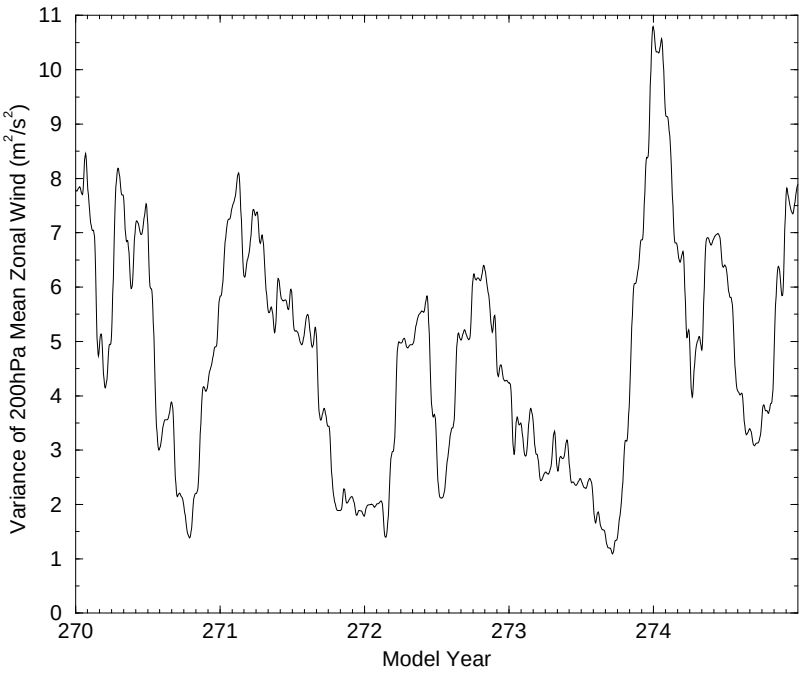


Figure 20: ECHAM4/OPYC3 $\overline{u_{200}}$-variance averaged between 10°N and 10°S within a 100-day moving window, an index for the interannual variability of the MJO activity.

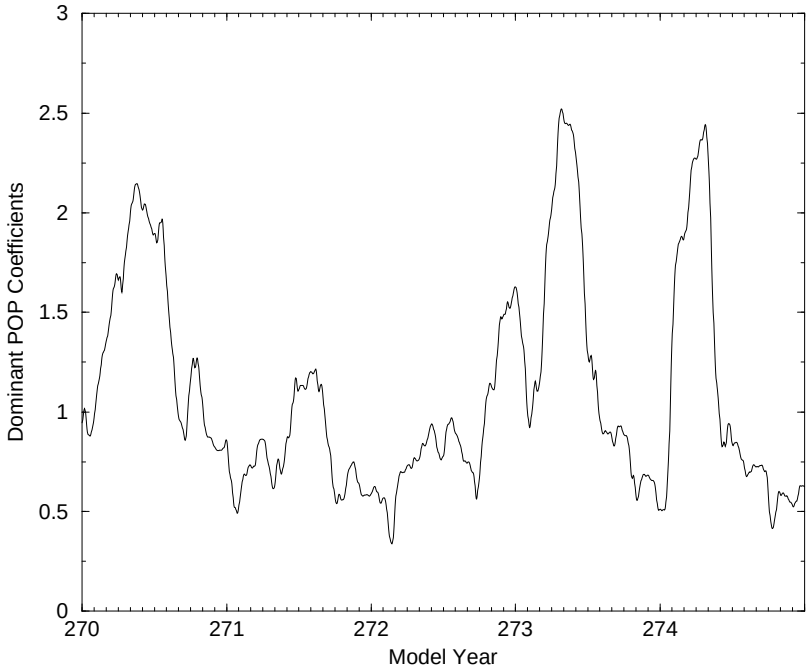


Figure 21: ECHAM4/OPYC3 100-day running mean of the squared amplitude of the POP coefficients, reflecting the interannual variability of the MJO activity.

The following paragraphs describe the MJO event in year 274 of the simulation. A comparison of the model's wind field to the observations from Singapore (Fig. 10) shows that the MJO is not properly described in this respect. Fig. 22 shows the equatorial zonal wind at 200 hPa and 850 hPa and at 80°E and 140°E. These longitudes include the strongest variance of 200 hPa velocity potential and represent the centers of the two super cloud clusters as presented in Fig. 17. The mean 200 hPa easterlies are less apparent in the model, and the response of the lower tropospheric zonal wind is rather weak at the end of March. Further, the time series of upper- and low-level zonal winds are not well correlated.

Beneath the erroneous gap of convection over the maritime continent we find an underestimation of low- and mid-level clouds (Fig. 23) compared to the reanalysis (Fig. 11). The mid-level convection scheme in the model represents the wave-CISK mechanism (ECMWF, 2000). The simulations by Lau et al. (1989) with prescribed heating showed that maximum convective heating between 500 and 700 hPa is important for the correct simulation of the wind field and the eastward propagation speed of the super cloud cluster. The simulated convection in the ECHAM4/OPYC3 model occurs in higher levels than in the observations and therefore cannot describe correctly the frictional wave-CISK mechanism as described in Salby et al. (1994). Wang and Rui (1990a) and Salby et al. (1994) suggest that frictional convergence at the equator in the planetary boundary layer plays a key role in the amplification of the disturbance. Although it is not clear how

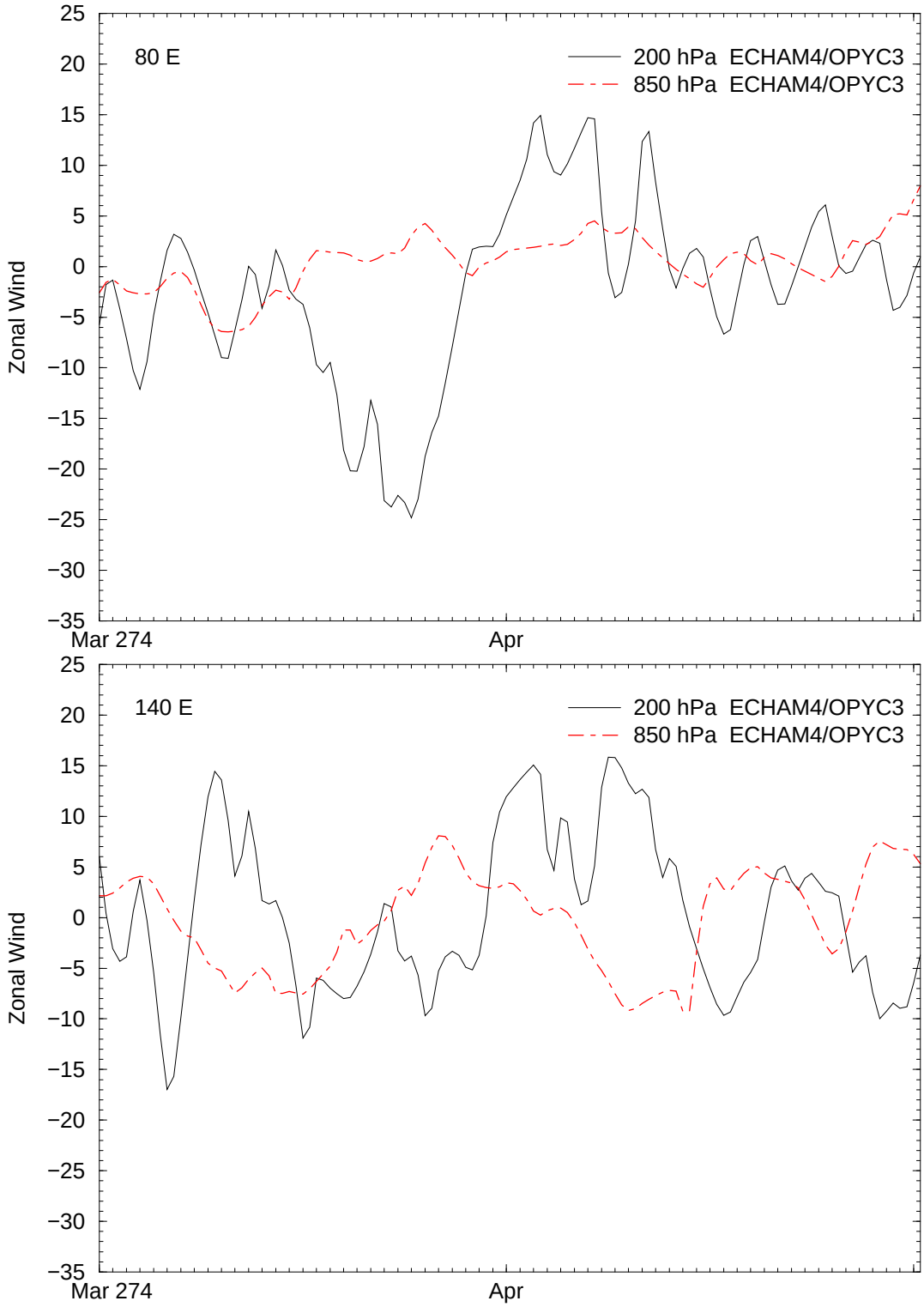


Figure 22: Time series of ECHAM4/OPYC3 equatorial zonal wind at 200 hPa (solid) and 850 hPa (dot dashed) and at 80°E (top) and 140°E (bottom). These grid points have the strongest variance of 200 hPa velocity potential and represent the centers of the two super cloud clusters.

significant the organization of convection in mesoscale rain bands is for the large-scale flow, a parametrization of mid-level convection should ideally account for both convective and mesoscale circulations. Such a parametrization, however, is presently not available (ECMWF, 2000).

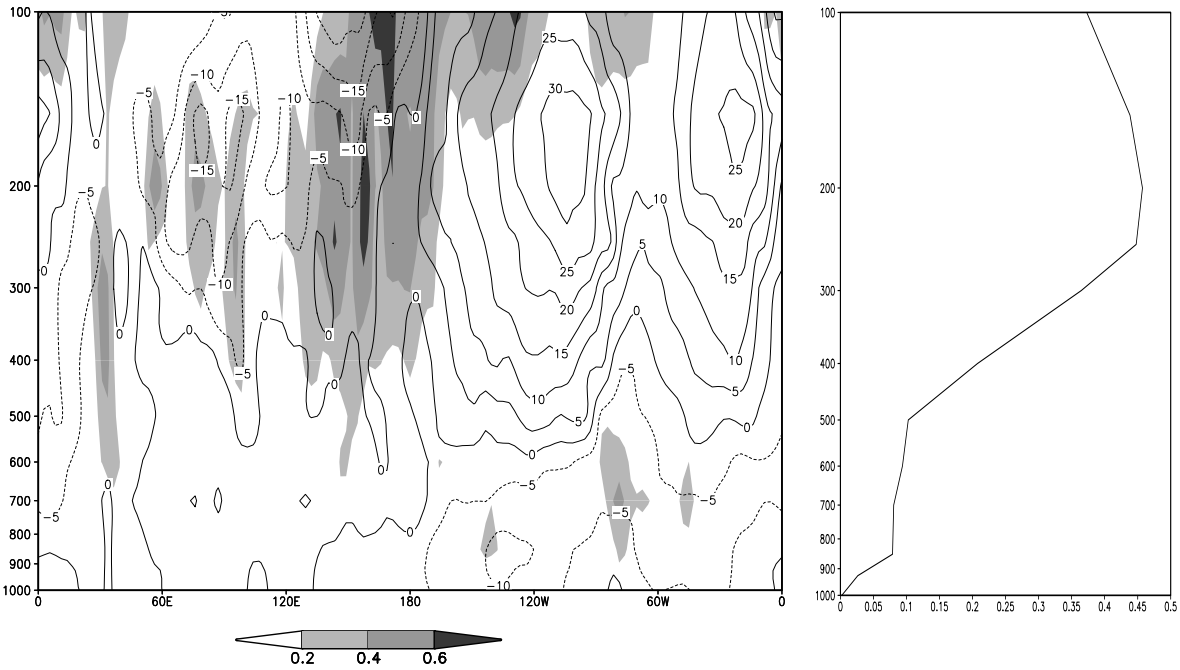


Figure 23: Same as Fig. 11, but for ECHAM4/OPYC3 data at March 24th 274.

Fig. 24 shows the time series of the model's NINO3 SSTA and the occurrence of the strong MJO event in the model. As in Fig. 8, the two vertical lines mark 20 days before and 40 days after the event, respectively. The simulated MJO occurs prior to a La Niña, at the time of steepest NINO3 SSTA decrease, as in the reanalysis data.

Longitude-time Hovmöller diagrams of the simulated MJO are compared to the respective diagrams of the satellite and reanalysis data. Fig. 25 depicts the OLR anomaly. Its variance is stronger than in the observations and the reanalysis data (Figs. 12), which is due to the fact that tropical convection reaches higher levels in the model (Fig. 23). As discussed above, the OLR anomaly is strongest and slows down too far east in the Central Pacific.

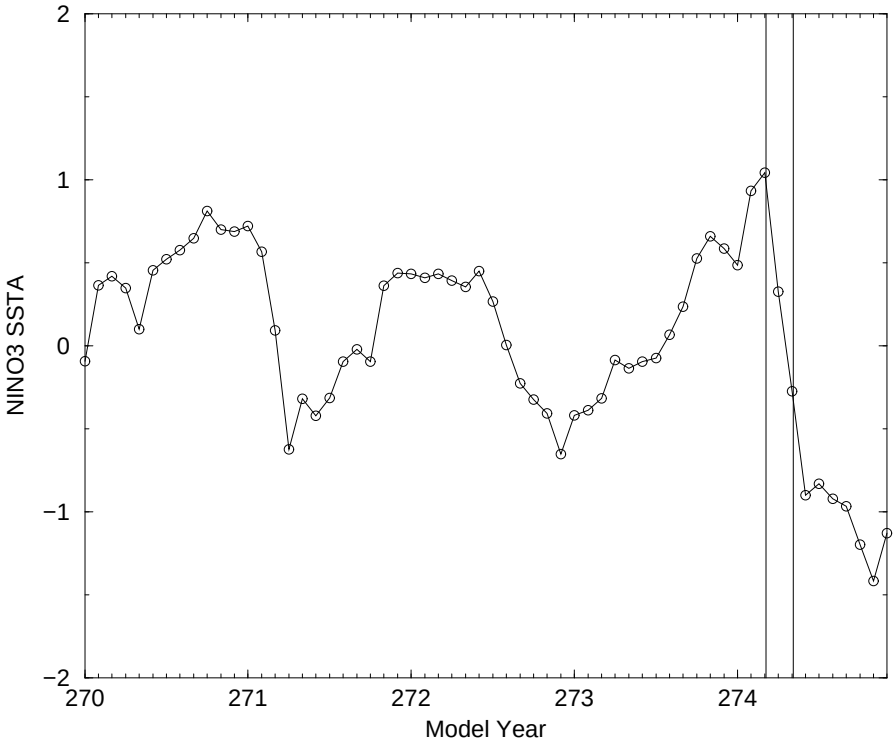


Figure 24: Comparison of NINO3 SSTA to the PC1 maximum with 20 days before and 40 days after the maximum indicated by the two vertical lines.

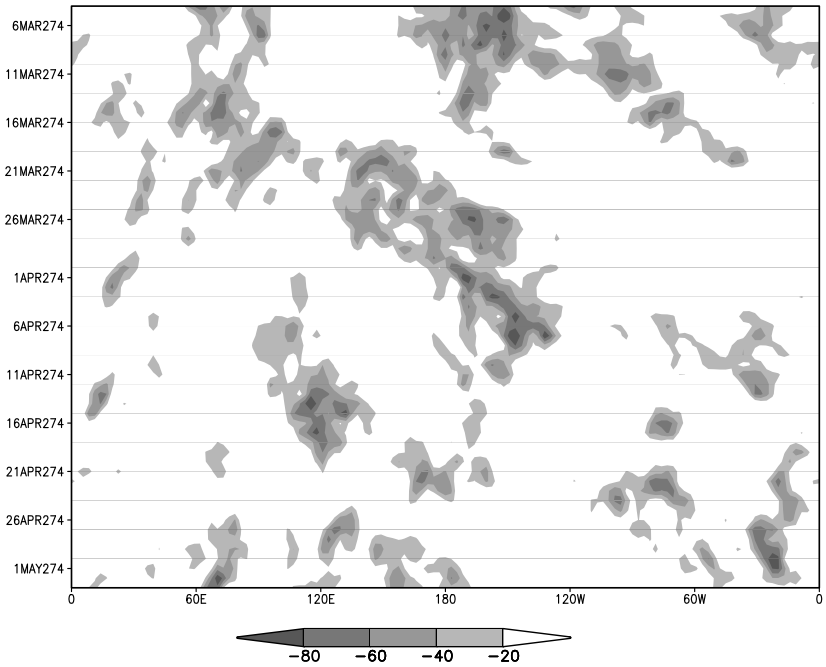


Figure 25: ECHAM4/OPYC3 OLR anomaly averaged between 10°N and 10°S.

The change of SST (Fig. 26) due to the passage of an MJO is of the same order as in the observations (Fig. 13). The cooling occurs at about 140°E and the warming takes place between 160°E and the dateline. The simulated 29.5 °C isotherm is too much confined to the equator in the Indian Ocean and shifted too much northward north of Australia. The warming in the Indian Ocean seems to be separated from the MJO event that occurs at the West Pacific warm pool by the relative cold land area of the maritime continent which is overrepresented in the coarse horizontal resolution of the model. A coupled model with horizontal resolution of T106 might improve the representation of SST in the maritime continent, but such a model experiment is not yet available.

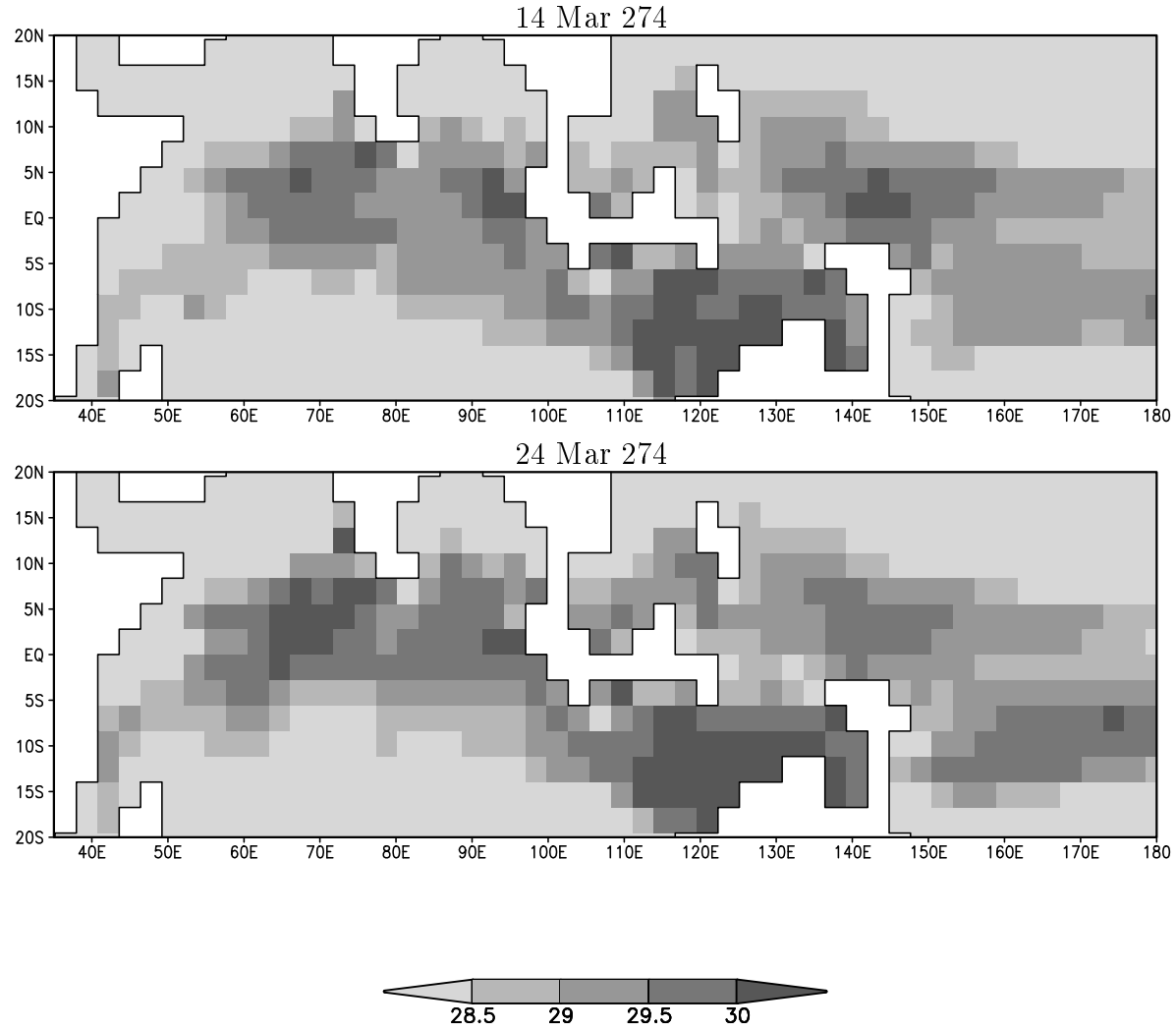


Figure 26: ECHAM4/OPYC3 SST [°C] with corresponding land-sea mask at March 14th (top) and March 24th (bottom) of model year 274.

The 200 hPa velocity potential anomaly (Fig. 27) propagates slightly too fast compared to the reanalysis data. It is temporally in phase with the 850 hPa velocity potential anomaly. The 850 hPa large-scale convergence slightly leads the 200 hPa large-scale divergence (eastward shift) spatially, which is consistent with the observations (e.g. Jones and Weare,

1996). The 1000 hPa and 925 hPa positive anomalies lag the 850 hPa anomaly slightly in time, which is consistent with the wave-CISK theory. The coupled model does simulate WWBs (Fig. 28) that result from the passage of MJOs. Their amplitudes, however, are relatively weak. The first WWB is stretched too far eastward as the low-level large-scale convergence in Fig. 27.

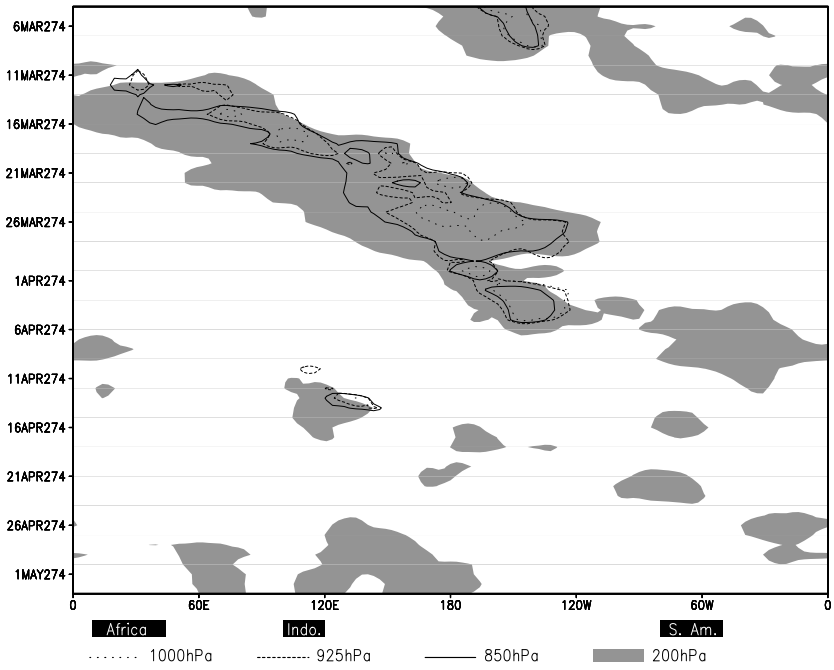


Figure 27: Same as Fig 14, but for ECHAM4/OPYC3.

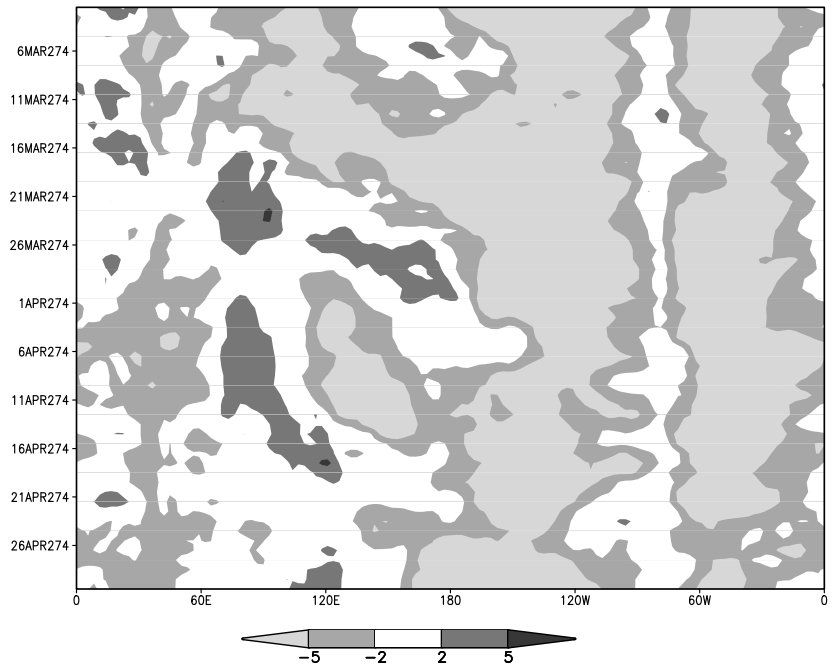


Figure 28: Same as Fig 15, but for ECHAM4/OPYC3.

# 4 Discussion of the results

The present study describes the capability of the ECHAM4/OPYC3 CGCM to simulate the MJO. A POP analysis reveals that the general features are well simulated, although the model suffers from a too short period of 27 days compared to 48 days in the reanalysis data and an eastward shift of the MJO activity due to the erroneous gap of convection over the maritime continent. These problems are common to GCMs (Slingo et al., 1996). A possible reason for the gap is the low horizontal resolution of the model with too much area in the maritime continent covered by land. This barrier with skin temperatures of more than 1 K below the surrounding sea stops the continuous moisture supply and is therefore responsible for the splitting of the super cloud cluster over the maritime continent, as will be shown in a forthcoming paper. The too strong convection over the South American rainforest in the model seems to reinforce the simulated MJO, which is indicated by the secondary maximum in 200hPa velocity potential anomaly.

In both data sets the strongest MJO events occur prior to a La Niña. This is probably due to the increased convective activity over the eastern Indian Ocean and the West Pacific warm pool. During the mature phase of La Niña during northern summer the ITCZ is shifted north of the equator, so that the deep convection occurs too far north of the equator to initiate equatorial Kelvin waves. Therefore the MJO activity decreases. The interannual variability is present in the model, but the main activity occurs too late in the year in spring and summer instead of winter and spring as observed.

A case study provides a lot of insight into the structure of the MJO, although it has to be kept in mind that this insight cannot be transfered to other MJO events. Averaging over many MJOs, however, might lead to deficient evidences when local disturbances are considered. The case study clarifies that the strong updrafts associated with the deep convection in the eastern hemisphere force the MJO. Convection and upper troposphere zonal wind field are in phase at this stage of the MJO. SST and convergence in the boundary layer lead this phase.

The coupled model is partially capable of representing the slight eastward shift of the low-level velocity potential anomaly, but the model convection does not allow the frictional wave-CISK mechanism to develop. This frictional wave-CISK mechanism is distinguished from classical wave-CISK, which is well represented in the model but gives preference to the long zonal waves (Salby et al., 1994). Another deficiency of the convection scheme is its inability to represent the trimodal vertical structure of cloud cover in the tropics. It does not support deep convection and mid-level convection at the same time at one horizontal grid point. Low- and mid-level convection is necessary to moisten the atmosphere whereas deep convection dries the atmosphere. Inness et al. (2001) claim that increasing the

vertical resolution from 19 to 30 layers is sufficient to obtain the trimodal structure of cloud cover. This improves the representation of the MJO in the Hadley Centre model. A study with the ECHAM4 AGCM with 39 layers will be presented in a forthcoming paper. The improvements of increased vertical resolution are pointed out by Tompkins and Emanuel (2000) for the ECHAM4 one-column model.

The deviation of SST and low-level large-scale convergence to the east and associated WWBs increase the latent heat flux closly to the west of the convection. They retard the propagation speed of the MJO in the Indian ocean and the West Pacific warm pool (Crum and Dunkerton, 1994; Jones and Weare, 1996). The initiated variations of SST and WWBs lead to an oceanic Kelvin wave (e.g. Zhang, 1997) that might influence the ENSO phenomenon (e.g. van Oldenborgh, 2000).

# 5 Conclusion

AGCMs have still many deficiencies in representing the MJO as shown in a model intercomparison by Slingo et al. (1996). Since the MJO is considered to be a coupled atmosphere-ocean phenomenon, the present study analyzes the occurrence of the MJO in the ECHAM4/OPYC3 CGCM. Although it has to be pointed out that the CGCM still reflects many weaknesses of the AGCMs, the interaction with the ocean mixed layer is well simulated. The SST varies between 0.1 and 0.5 K consistent with observations.

We conclude that an improvement of the parameterization of convection, e.g. the occurrence of mid-level convection, which represents the wave-CISK mechanism, is important for a better simulation of the MJO in GCMs. Other improvements can be gained by increasing the horizontal and vertical resolution of the GCM until the erroneous large extent of relative cold land surface at the maritime continent vanishes and the trimodal vertical structure of cloud cover can be represented, respectively.

# Acknowledgements

The authors would like to thank Dr. Silvio Gualdi, Pete M. Innes and the staff at MPI for helpful comments and discussions. The ECMWF made the radiosonde measurements at Singapore airport available as part of the MARS dataset. The reanalysis data were supplied by ECMWF and DWD in cooperation with DKRZ. The NOAA data were kindly provided by the CPC.

# References


Bacher, A., J. M. Oberhuber and E. Roeckner (1998): ENSO dynamics and seasonal cycle in the tropical Pacific as simulated by the ECHAM4/OPYC3 coupled general circulation model. *Climate Dyn.*, **14**, 431–450.

Crum, F. X. and T. J. Dunkerton (1994): CISK and evaporation-wind feedback with conditional heating on an equatorial beta-plane. *J. Meteor. Soc. Japan*, **72**, 11–18.

ECMWF (2000): *IFS Documentation (CY21r4)*. http://www.ecmwf.int/research/ifsdocs.

Emanuel, K. A. (1987): Air-sea interaction model of intraseasonal oscillations in the Tropics. *J. Atmos. Sci.*, **44**, 2324–2340.

Flatau, M., P. J. Flatau, P. Phoebus and P. P. Niiler (1997): The feedback between equatorial convection and local radiative and evaporative processes: The implications for intraseasonal oscillations. *J. Atmos. Sci.*, **54**, 2373–2386.

Gallagher, F., H. von Storch, R. Schnur and G. Hannoschoeck (1991): The POP manual. Technical Report 1, Deutsches Klimarechenzentrum, Hamburg, Germany. 66 pp.

Gualdi, S., A. Navarra and G. Tinarelli (1999): The interannual variability of the Madden-Julian oscillation in an ensemble of GCM simulations. *Climate Dyn.*, **15**, 643–658.

Gualdi, S., A. Navarra and H. von Storch (1997): Tropical intraseasonal oscillation appearing in operational analysis and in a family of general circulation models. *J. Atmos. Sci.*, **54**, 1185–1202.

Hasselmann, K. (1988): PIPs and POPs: The reduction of complex dynamical systems using principal interaction and oscillation pattern. *J. Geophys. Res.*, **93**, 11015–11021.

Hayashi, Y.-Y. and D. G. Golder (1993): Tropical 40-50- and 25-30-day oscillations appearing in realistic and idealised GFDL climate models and the ECMWF dataset. *J. Atmos. Sci.*, **50**, 464–494.

Hayashi, Y.-Y. and A. Sumi (1986): The 30-40-day oscillations simulated in an "aqua planet" model. *J. Meteor. Soc. Japan*, **64**, 451–467.

Hendon, H. H. and B. Liebmann (1990a): A composite study of onset of the Australian summer monsoon. *J. Atmos. Sci.*, **47**, 2227–2240.

Hendon, H. H. and B. Liebmann (1990b): The intraseasonal (30-50 day) oscillation of the Australian summer monsoon. *J. Atmos. Sci.*, **47**, 2909–2923.

Hendon, H. H., B. Liebmann, M. Newman, J. D. Glick and J. E. Schemm (2000): Medium-range forecast errors associated with active episodes of the Madden-Julian oscillation. *Mon. Wea. Rev.*, **128**, 69–86.

Inness, P. M., J. M. Slingo, S. J. Woolnough and R. B. Neale (2001): Organization of tropical convection in a GCM with varying vertical resolution; implications for the simulation of the Madden-Julian oscillation. *Climate Dyn.*, accepted.

Johnson, R. H., T. M. Rickenbach, S. A. Rutledge, P. E. Ciesielski and W. H. Schubert (1999): Trimodal characteristics of tropical convection. *J. Climate*, **12**, 2397–2418.

Jones, C., D. E. Waliser and C. Gautier (1998): The influence of the Madden-Julian oscillation on ocean surface heat fluxes and sea surface temperature. *J. Climate*, **11**, 1057–1072.

Jones, C. and B. C. Weare (1996): The role of low-level moisture convergence and ocean latent heat fluxes in the Madden-Julian oscillation: An observational analysis using ISCCP data and ECMWF analyis. *J. Climate*, **9**, 3086–3104.

Kessler, W. S., M. McPhaden and K. M. Weickmann (1995): Forcing of intraseasonal Kelvin waves in the equatorial Pacific. *J. Geophys. Res.*, **100**, 10613–10631.

Knutson, T. R. and K. M. Weickmann (1987): 30-60 day atmospheric oscillations: Composite life cycles of convection and circulation anomalies. *Mon. Wea. Rev.*, **115**, 1407–1436.

Krishnamurti, T. N., D. K. Oosterhof and A. V. Mehta (1988): Air-sea interaction on the time scale of 30 to 50 days. *J. Atmos. Sci.*, **45**, 1304–1322.

Lau, K.-M. and F. C. Chang (1992): Tropical intraseasonal oscillation and its prediction by the NMC operational model. *J. Climate*, **5**, 1365–1378.

Lau, K.-M. and L. Peng (1987): Origin of low-frequency (intraseasonal) oscillations in the tropical atmosphere. Part I: Basic theory. *J. Atmos. Sci.*, **44**, 950–972.

Lau, K.-M., L. Peng, C.-H. Sui and T. Nakazawa (1989): Dynamics of super cloud clusters, westerly wind bursts, 30-60-day oscillations, and ENSO: a unified view. *J. Meteor. Soc. Japan*, **67**, 205–219.

Lau, K.-M. and C.-H. Sui (1997): Mechanisms of short-term Sea Surface Temperature regulation: Observations during TOGA COARE. *J. Climate*, **10**, 465–472.

Liebmann, B. and C. A. Smith (1996): Description of a complete (interpolated) outgoing longwave radiation dataset. *Bull. Amer. Meteor. Soc.*, **77**, 1275–1277.

Lindzen, R. S. (1974): Wave-CISK in the tropics. *J. Atmos. Sci.*, **31**, 156–179.

Madden, R. A. and P. R. Julian (1971): Detection of a 40-50 day oscillation in the zonal wind in the tropical Pacific. *J. Atmos. Sci.*, **28**, 702–708.

Madden, R. A. and P. R. Julian (1972): Description of global-scale circulation cells in the ropics with a 40-50 day period. *J. Atmos. Sci.*, **29**, 1109–1123.

Madden, R. A. and P. R. Julian (1994): Observations of the 40-50-day tropical oscillation - a review. *Mon. Wea. Rev.*, **122**, 814–837.

Matsuno, T. (1966): Quasi-geostrophic motions in the equatorial area. *J. Meteor. Soc. Japan*, **44**, 25–43.

Matthews, A. J., B. J.Hoskins, J. M. Slingo and M. Blackburn (1996): Developement of convection along the SPCZ within a Madden-Julian oscillation. *Quart. J. Roy. Meteor. Soc.*, **122**, 669–688.

McPhaden, M. J. and B. A. Taft (1988): Dynamics of seasonal and intraseasonal variability in the eastern equatorial Pacific. *J. Phys. Oceanogr.*, **18**, 1713–1732.

Nakazawa, T. (1999): MJO–a key component in the atmosphere for triggering ENSO. In: *Conference on the TOGA Coupled Ocean-Atmosphere Response Experiment (COARE), Boulder, Colorado, USA, 7-14 July 1998, COARE-98*. Geneva, Switzerland, World Meteorological Organization, WMO/TD 940, pp. 165–166.

Neelin, J. D., I. M. Held and K. H. Cook (1987): Evaporation-wind feedback and low-frequency variability in the tropical atmosphere. *J. Atmos. Sci.*, **44**, 2341–2348.

Philander, S. G. (1990): *El Niño, La Niña and the Southern Oscillation*. Academic Press. 293 pp.

Philander, S. G. H., D. Gu, D. Halpern, G. Lambert, N.-C. Lau, T. Li and R. C. Pacanowski (1996): Why the ITCZ is mostly north of the equator. *J. Climate*, **9**, 2958–2972.

Picaut, J. and T. Delcroix (1995): Equatorial wave sequence associated with warm pool displacements during the 1986-1989 El Nino-La Nina. *J. Geophys. Res.*, **100**, 18393–18408.

Roeckner, E., J. M. Oberhuber, A. Bacher, M. Christoph and I. Kirchner (1996): ENSO variability and atmospheric response in a global coupled atmosphere-ocean GCM. *Climate Dyn.*, **12**, 737–754.

Rui, H. and B. Wang (1990): Development characteristics and dynamic structure of tropical intraseasonal convection anomalies. *J. Atmos. Sci.*, **47**, 357–379.

Salby, M. L., R. R. Garcia and H. H. Hendon (1994): Planetary-scale circulations in the presence of climatological and wave-induced heating. *J. Atmos. Sci.*, **51**, 2344–2367.

Salby, M. L. and H. H. Hendon (1994): Intraseasonal behavior of clouds, temperature, and motion in the tropics. *J. Atmos. Sci.*, **51**, 2207–2224.

Slingo, J. M., D. P. Rowell, K. R. Sperber and F. Nortley (1999): On the predictability of the interannual behaviour of the Madden-Julian oscillation and its relationship with El Niño. *Quart. J. Roy. Meteor. Soc.*, **125**, 583–609.

Slingo, J. M., K. R. Sperber, J. S. Boyle, J.-P. Ceron, M. Dix, B. Dugas, W. Ebisuzaki, J. Fyfe, D. Gregory, J.-F. Gueremy, J. Hack, A. Harzallah, P. Inness, A. Kitoh, W. K.-M. Lau, B. McAvaney, R. Madden, A. Matthews, T. N. Palmer, C.-K. Park, D. Randall and N. Renno (1996): Intraseasonal oscillations in 15 atmospheric general circulation models: Results from an AMIP diagnostic subproject. *Climate Dyn.*, **12**, 325–357.

Swinbank, R., T. N. Palmer and M. K. Davey (1988): Numerical simulations of the Madden and Julian oscillation. *J. Atmos. Sci.*, **45**, 774–788.

Tompkins, A. M. and K. A. Emanuel (2000): The vertical-resolution sensitivity of simulated equilibrium tropical temperature and water-vapor profiles. *Quart. J. Roy. Meteorol. Soc.*, **126**, 1219–1238.

van Oldenborgh, G. J. (2000): What caused the 1997-1998 El Niño? *Mon. Wea. Rev.*, **128**, 2601–2607.

von Storch, H., T. Bruns, I. Fischer-Bruns and K. Hasselmann (1988): Principal oscillation pattern analysis of the 30- to 60-day oscillation in general circulation model equatorial troposphere. *J. Geophys. Res.*, **93**, 11022–11036.

von Storch, H., G. Bürger, R. Schnur and J. von Storch (1995): Principal oscillation patterns: A review. *J. Climate*, **8**, 377–400.

von Storch, H. and F. W. Zwiers (1999): *Statistical Analysis in Climate Research*. Cambridge University Press, Cambridge. 550 p.

Waliser, D. E., K. M. Lau and J.-H. Kim (1999): The influence of coupled Sea Surface Temperatures on the Madden-Julian oscillation: A model perturbation experiment. *J. Atmos. Sci.*, **56**, 333–358.

Wang, B. (1988): Dynamics of tropical low-frequency waves: An analysis of the moist Kelvin waves. *J. Atmos. Sci.*, **45**, 2051–2065.

Wang, B. and H. Rui (1990a): Dynamics of the coupled moist Kelvin-Rossby wave on an equatorial $\beta$-plane. *J. Atmos. Sci.*, **47**, 397–413.

Wang, B. and H. Rui (1990b): Synoptic climatology of transient tropical intraseasonal convection anomalies. *Meteor. Atmos. Phys.*, **44**, 43–61.

Wang, B. and X. Xie (1998): Coupled modes of the warm pool climate system. Part I: The role of air-sea interaction in maintaining Madden-Julian oscillation. *J. Climate*, **11**, 2116–2133.

Weickmann, K. M. (1991): El Nino/Southern Oscillation and Madden-Julian (30-60 day) oscillations during 1981-1982. *J. Geophys. Res.*, **96**, 3187–3195.

Wheeler, M., G. N. Kiladis and P. J. Webster (2000): Large-scale dynamical fields associated with convectively coupled equatorial waves. *J. Atmos. Sci*, **57**, 613–640.

Zhang, C. (1997): Intraseasonal variability of the upper-ocean thermal structure observed at 0 degrees and 165 degrees E. *J. Climate*, **10**, 3077–3092.

Zhang, C. and H. H. Hendon (1997): Propagating and standing components of the intraseasonal oscillation in tropical convection. *J. Atmos. Sci.*, **54**, 741–752.